Univerzita Karlova v Praze
Matematicko-fyzikální fakulta

# DIPLOMOVÁ PRÁCE

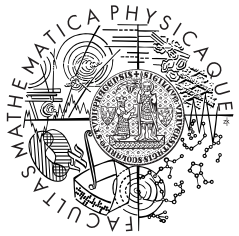


Jan Linhart

## Nelineární optická spektroskopie molekulárních komplexů

Fyzikální ústav UK

Vedoucí práce: RNDr. Tomáš Mančal, Ph.D.

Studijní program: Biofyzika a chemická fyzika

2011

Chtěl bych vyjádřit poděkování svému vedoucímu Tomáši Mančalovi za neocenitelnou a nesmírně vytrvalou pomoc, kterou mi během psaní mé diplomové práce poskytl. Vážím si jeho přístupu, který k diplomantům (a nejen k nim) zaujímá. Zároveň děkuji Janu Olšinovi, bez jehož pomoci bych se jen těžko prokousával složitosmi programového balíku NOSE.

Prohlašuji, že jsem svou diplomovou práci napsal samostatně a výhradně s použitím citovaných pramenů. Souhlasím se zapůjčováním práce a jejím zveřejňováním.

V Praze dne Jméno Příjmení

# Contents

Název práce: Nelineární optická spektroskopie molekulárních komplexů
Autor: Jan Linhart
Katedra: Fyzikální ústav UK
Vedoucí diplomové práce: RNDr. Tomáš Mančal, Ph.D.
Email vedoucího: mancal@karlov.mff.cuni.cz

Abstrakt: Práce se zabývá teorií nelineární spektroskopie a projevy kvantové koherentní dynamiky v nelineární spektroskopii. Poskytuje stručný přehled spektroskopických metod se zaměřením na metodu pump-probe. Dále rozvíjíme teorii nelineární odezvy, přičemž vycházíme z obecného N-wave mixing experimentu, a dospíváme ke tvaru odezvové funkce třetího řádu vyjádřené pomocí Liouvillových drah. Pro vybrané modelové systémy sledujeme koherentní efekty, které se projevují v 2D a pump-probe spektrech, a provádíme jejich porovnání. Důraz je kladen na objasnění jevů relaxace a excitonové koherence mezi dvěma excitovanými stavy molekulárního dimeru.

Klíčová slova: pump-probe, 2D spektroskopie, nelineární spektroskopie, odezvové funkce, Liouvillovy dráhy

Title: Nonlinear optical spectroscopy of molecular complexes
Author: Jan Linhart
Department: Institute of Physics
Supervisor: RNDr. Tomáš Mančal, Ph.D.
Email address: mancal@karlov.mff.cuni.cz

Abstract: This thesis deals with the theory of non-linear spectroscopy and effects of coherent quantum dynamics in non-linear spectroscopy. It provides a short review of spectroscopic methods with an emphasis on the pump-probe technique. Studying general process of N-wave mixing experiment, we develop a theory of non-linear response and in terms of Liouville pathways we derive the mathematical expression for 3rd order response function. We present examples of manifestations of coherent effects in 2D and pump-probe spectra and their comparison. Special attention is paid to relaxation and exciton coherence between two excited electronic states of a molecular dimer.

Keywords: pump-probe, 2D spectroscopy, nonlinear spectroscopy, response functions, Liouville pathways

# Chapter 1

# Introduction

First of all, let me introduce my personal motivation. This work should be a continuation of my creative efforts in the field of non-linear spectroscopy which I started a few years ago in my Bachelor's thesis. My goal then was mainly to get familiar with basic principles and to make the first steps to become a specialist in that field. But it was not my original intention to do what I do now. Instead, I feel it was rather the process of photosynthesis that attracted my attention. However, it did not take much time to realize, that it is the spectroscopy that is able to give answers when we ask for the mechanisms that are behind such complex molecular processes. Therefore, I started to learn about such things as Redfield theory, superoperator formalism or exciton theory and in the same time I was also able to learn about the primary processes of photosynthesis on far deeper level than I did ever before. And maybe most importantly I got familiar with various spectroscopic methods that are used in modern spectroscopy, especially with the pump-probe technique. On a purely phenomenological level I (with help of my supervisor) managed to create a model which allowed me to study dynamics and relaxation processes that take place in bacterial photosynthetic reaction centers. And when I obtained results that were quantitatively correct I was thrilled. "This is something that I have been studying for," I said to myself and it became an inspiration for me to try and do even more.

In this thesis, the main role plays the pump-probe technique. We tried to achieve three goals. Firstly, the second chapter summarizes some fundamental facts about spectroscopy in general, it also gives short description about a few chosen spectroscopic methods providing high resolution with the main emphasis on describing all possible aspects of pump-probe technique, its es-

sential characteristics and applications. Secondly, we decided to properly formulate the theory that underlies the detection of non-linear optical signals and to derive the form of Liouville pathways which play the crucial role in pulsed experiments such as fluorescence up-conversion, pump-probe or 2D spectroscopy. This is the content of the third chapter. Finally, in the fourth chapter we present our simulations that we obtained using the spectroscopic program NOSE, while we focused on describing differences and similarities between pump-probe and 2D.

# Chapter 2

# Spectroscopy

Today, talking about spectroscopy means to take in consideration many various fields of study and many both simple and advanced theoretical principles and experimental instrumentation. Vaguely speaking, spectroscopy concerns the matter-radiation interaction which may provide experimentators with large amount of information about the studied system. On the molecular level this information could be for example about the common properties such as excited states energy, transition dipole moment etc., or about dynamics (excited states lifetime etc.). Through spectroscopy one may also reveal conformation of a molecule, or even its function in a biological system. The use of spectroscopy in biology, chemistry, and material studies is nowadays quite common, because there is usually no other way to look into the system on the molecular level.

In our work we specialize on recently developed modern type of experiments, which are pump-probe, 2D spectroscopy and general N-wave mixing non-linear experiments. In contrast to spectroscopy high resolution microscopes like AFM (Atomic Force Microscope) or MFM (Magnetic Force Microscope) capable of scanning matter on the order of fractions of a nanometer are extremely useful in determining atomic structure or inter-atomic forces including electrostatic forces, atomic forces, Van der Waals forces and chemical bonding. Nevertheless, there is another very ordinary field which depends on our knowledge about radiation transfer, origin, and interaction, and this is cosmology. And we must not forget that understanding of light-matter interactions also plays an undoubted role in scientific description of the process of seeing, structure of an eye.

Every spectroscopic experiment provides us with some kind of spectrum.

The nature of each spectrum is determined by the nature of preceding experiment. There is a vast range of types of spectra and every one of them differs a little from each other. Some of them are two-dimensional whereas others are three-dimensional, that is mostly when time-dependence is covered.

Probably the most fundamental experiment one can think of is the determination of the frequency dependent absorption curve of a material. This could be done by using two beams of radiation, the measuring one and the reference one. While the reference beam passes along the sample, the measuring beam goes right through it. By comparing the final intensities of these two beams we are able to find out how big portion of radiation has been absorbed.

Let us say that the intensity of the reference beam as it reaches a detector is $I_0(\omega)$ and similarly the intensity of the measuring beam is $I(\omega)$. By taking the fraction of these two values we obtain the physical quantity called transmittance

$$T(\omega) = \frac{I(\omega)}{I_0(\omega)}. \tag{2.1}$$

Instead, we may also use absorbance $A(\omega)$, which is defined as a negative value of decadic logarithm of transmittance, i.e.

$$A(\omega) = -\log T(\omega) \tag{2.2}$$

It is a very important quantity because it appears in Lambert-Beer's law which states that the absorbance of a sample is directly proportional to the concentration of the sample in a solution which is a property of great significance

$$A(\omega) = \varepsilon(\omega)cd. \tag{2.3}$$

Here we see that the only three values that we need to know in order to determine the absorbance $A(\omega)$ of a sample are the molar **extinction coefficient** $\varepsilon(\omega)$ which is tabulated for many materials, the thickness of a sample $d$ and finally its concentration $c$. As we can see in this situation we would get an exact absolute value of $A(\omega)$ but despite of that in many other cases just the overall profile of the absorption curve is sufficient enough. It always depends on the goal we are trying to achieve.

Let us briefly turn our attention to the absorption spectrum at this point. What does its shape tell us about the material? First of all there is information about the transitions between energy levels of the sample. We may assume for a moment that there is an infinitely narrow single absorption line

in an absorption spectrum at the exact frequency $\omega$. This would lead to the conclusion that there exists an optical transition in the system given by the energy difference of $\hbar\omega$ and that only photons carrying this particular energy are absorbed. Of course, real spectrum comprises lines with certain widths. Naturally broadened lines have lorentzian shape which could be written as[1]

$$L(\omega) = \frac{1}{2\pi} \frac{\gamma}{(\omega - \omega_0)^2 + (\gamma/2)^2}, \tag{2.4}$$

where $\omega_0$ is the position of the maximum on a frequency axis and $\gamma$ is full width at half maximum (FWHM). This particular form obeys the normalization condition

$$\int_{-\infty}^{\infty} L(\omega) \mathrm{d}\omega = 1. \tag{2.5}$$

There is also another widely used form of natural line-shape

$$L(\omega) = \frac{\Gamma^2}{(\omega - \omega_0) + \Gamma^2}, \tag{2.6}$$

where $\Gamma = \gamma/2$. It is the Lorentz function as well but this time the normalization is chosen so that $L(\omega_0) = 1$. In the former case $L(\omega_0)$ would be $2/\pi\gamma$.

At this point we can summarize that every absorption line is defined by its shape, height and width. For a lorentzian line-shape we get a simple connection between its width and excited state lifetime $\tau$

$$\mathrm{FWHM} = 1/\tau. \tag{2.7}$$

This means that if an excited state of a molecule had an infinite lifetime the width of its absorption line would be zero. This is never the case though. On account of that let us take a brief but a little closer look into possible line-shapes. Both definitions (2.4) and (2.6) apply for so called natural line-shapes. What does it mean? It means that no external conditions are taken into consideration. As the intention of this work is to concentrate mostly on absorption in biological materials let us for example say we are interested in the absorption spectrum of some chlorophyll pigment molecule. The most straightforward extension of our investigative efforts would be to include so called *bath*, the natural environment of absorbing molecule. We

[1] Definitions of line-shapes as well as some examples of broadening mechanisms were taken from reference [12], chapter 3 "Widths and profiles of spectral lines".

make it possible for the molecule to exchange energy with it. The energy of the excited state is dissipated more quickly and a lifetime of an excited state becomes shorter. With regard to the connection between the lifetime of an excited state and the width of the absorption line the result of just described effect is a spectral line broadening. Mathematically we can write that $\tau$ from (2.7) becomes $\tau_1$ while $\tau_1 < \tau$. $\tau_1$ is **dephasing time** caused by **relaxation**. Because of electrostatic and Van der Waals forces molecule-bath interaction may also cause some deformation in the molecule's structure and thus change the frequency of a photon molecule absorbs[2]. These forces may be as well seen as a reason for line broadening and for that purpose there is a special function $\tau_2(T)$ associated with this effect. $\tau_2(T)$ is called **pure optical dephasing time** and is a function of temperature $T$. In this case FWHM would read

$$\text{FWHM} = \gamma = \frac{1}{\tau\prime} = \frac{1}{\tau_1} + \frac{1}{\tau_2(T)} \tag{2.8}$$

This result could be of course derived theoretically using density matrix and simple two-level system model.

Summarizing previous ideas we can present a unique definition which says that homogeneously broadened lines have those transitions whose probability of absorption or emission of radiation is equal for all the molecules of a sample. In other words if a photon with frequency $\omega$ causes a transition from ground to one of the excited states for one molecule of a sample with probability $P$ then after absorbing another photon of the same frequency $\omega$ the very same transition will occur with the exactly same probability $P$ for any other molecule of the sample. Natural line broadening is a special case of homogeneous broadening. On the other hand when the probability of absorption or emission is not equal for all molecules and is rather given by some kind of distribution function, we talk about *inhomogeneous line broadening*. An example of such broadening is Doppler broadening which applies to gaseous samples. Molecules of gas travel through space with a given velocity that obeys Maxwell distribution of speed. Let us say we choose a small group of molecules whose velocity component lies within the interval $(v_z, v_z + \Delta v_z)$. These molecules would be absorbing or emitting radiation with a frequency $\omega = \omega_0 + v_z k$ where $\omega_0$ stands for absorption frequency of steady molecules and $k$ is the absolute value of wave vector of radiation. Next we define $\gamma_n$ to be $\Delta v_z k$. $\gamma_n$ may be considered to be a frequency

[2]Such a shift in frequency is also referred to as *solvent shift*.

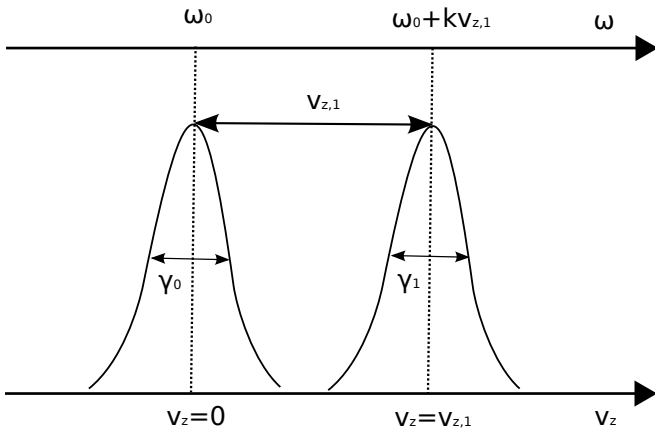


Figure 2.1: Doppler effect causing inhomogeneous broadening. The picture shows two homogeneous lines each corresponding to a different subgroup of molecules moving with a certain velocity.

interval (FWHM) of homogeneously broadened line belonging to the chosen group of molecules inside much larger inhomogeneously broadened line of all molecules of gas. For better understanding of the effect see the illustrative Fig. 2.1.

Another example of inhomogeneous broadening, and this time closer to study of biological materials, might be a sample localized inside an amorphous material or a real crystal lattice where each molecule is surrounded by slightly different environment (static disorder) that influences the value of transition energy and thus makes the line inhomogeneous. In a perfect crystal no such effect could be observed.

## 2.1 High resolution methods in spectroscopy

With a constantly increasing quality of spectroscopic instrumentation and mostly with the invention of lasers few decades ago, it has gradually become possible to study molecular systems with a great degree of precision. In other words, spectral resolution increases. However, high spectroscopic resolution does not have to be necessarily connected only to a better sensitivity in frequencies, it may also refer to an improved resolution in time domain. In high resolution spectroscopy it is always either time or frequency that is taken into account, since there is no way to perform a measurement where

the data output sensitivity would be comparable in both domains. Generally we have

$$\Delta t \Delta \nu \geq 1 \tag{2.9}$$

with $\Delta t$ being the pulse duration and $\Delta \nu$ denoting a spectral bandwidth (FWHM). For Gaussian-shape we may specify this inequality and come to the form

$$\Delta t \Delta \nu \doteq 0.44 \tag{2.10}$$

This relation known as **time-bandwidth product** is essentially a property of the Fourier transform and for a given spectral width it sets strict lower limit for the pulse duration. For instance, a 10-fs pulse has a spectral bandwidth (FWHM) of 4.4 $\times 10^{13}$ Hz for wavelength 100 nm.

Of course, this may cause some considerable difficulties while preparing an experiment for a concrete system where for some reason we need to use a laser pulse to excite only a certain part of absorbing molecules. Let us for example imagine an absorption spectrum with three absorption bands at 760 nm, 800 nm and 860 nm[3]. As in these days to generate as short laser pulses as 10 fs, or even shorter, is a common thing, we are allowed to achieve a very high time resolution since in pulsed experiments the resolution is usually given merely by the duration of the pulse. And that is the point where we have to choose, because if we decided to apply 10 fs pulse to the mentioned system we would excite all of the three absorption bands simultaneously. In order to selectively excite just a single type of molecules to study its excited-state dynamics, spectral narrowing to about 30 nm is required, which implies longer excitation pulse of the approximate duration of 30 fs. In many delicate cases the excitation bandwidth has to be narrowed even more (to less than 10 nm) for selective excitation. The corresponding pulse duration is then somewhere around 100 fs.

What has been said above suggests that spectroscopic methods are better to be split into two fields where one of them will emphasize mostly on achieving sufficient time resolution whereas the other one will stress on better frequency/ or wavelength precision. That is what we have done here, we divided high resolution spectroscopy on time and frequency domain and will list a few interesting (but not necessarily most important) methods that are used in modern science.

[3]These are quite common values that are in agreement with a standard absorption spectrum of the bacterial photosynthetic reaction center consisting of a special pair, accessory bacteriochlorophyls and bacteriopheophytines, each absorbing at slightly different wavelengths.

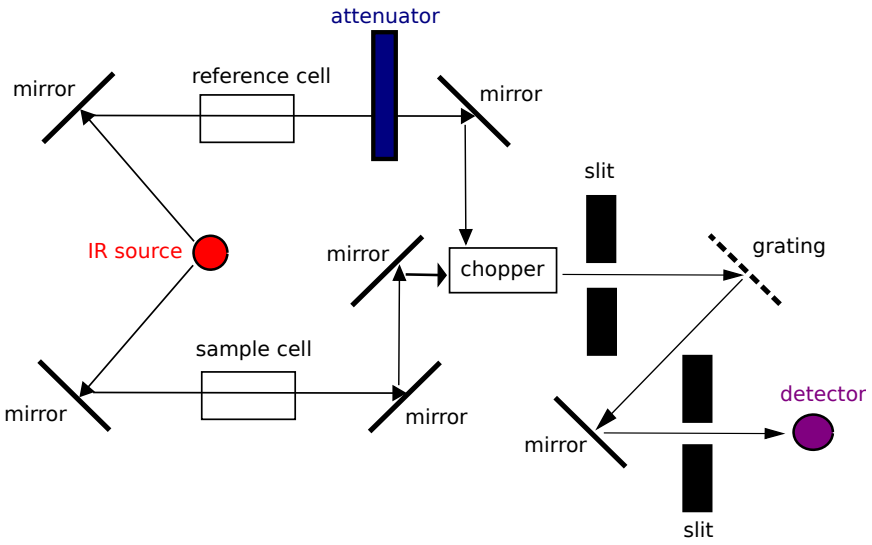


Figure 2.2: Grating infrared spectrometer

### 2.1.1 Frequency domain

**High resolved infrared spectroscopy**

Spectroscopic experiments are often similar for different spectral regions. The only thing one has to have on mind when doing experiments in infrared (IR) region is to use proper materials as the optical components of an infrared spectrometer have to be transparent to IR light. The nature of obtained spectra differs in each spectral area, those from ultraviolet and visible parts are associated with electronic transitions while absorption in IR occurs at frequencies where radiation energy correspond to vibrational or rotational energy levels of the molecule. Electronic transitions energy ($\sim 15\,000\,\mathrm{cm}^{-1}$) is typically by two orders of magnitude higher then that of vibrational transitions ($\sim 500\,\mathrm{cm}^{-1}$) and those of molecular rotations are even much lower. This calls for a need of sufficiently high resolution since if it was too low the vibrational peaks would join into one absorption band.

In principle there are two standard approaches to this task but nowadays one of them almost entirely overshadowed the other one. The first and more straightforward approach is based on a sequential scanning of intensities for all frequencies in spectrum. The instruments working in such a mode are called dispersive instruments. We will shortly describe the mechanisms of the simple *grating infrared spectrometer*. Light from the IR source is divided

into two beams, the first one is lead to a reference cell and the second to the sample cell. The reference beam is attenuated and then both beams go to the chopper, which is constructed so that it alternately allows light to pass from the reference cell to the grating and then light from the sample cell to the grating. At the grating light of a specific frequency is selected to pass to the IR detector. The whole mechanism is equipped with a controlling system that adjusts intensity of light coming from the reference cell, i.e. the degree of attenuation. The conditions are eventually set so that the intensity of both beams are identical. The amount of light absorbed is indicated by the position of the attenuator. The illustration of grating infrared spectrometer is shown in the Fig. 2.2. We did not yet mention its one last part, the slit. Its importance lies in the fact that by alternating its width, which is adjustable, one is able to control the resolution. However, the key role for us plays the element of grating mechanism that allow to measure only one particular wavelength at the time. This of course becomes increasingly time-consuming when one desires to achieve higher resolutions since in that case more and more steps have to be made. This little problem could be solved (and not only this one) by applying the method of acquiring spectra through the process of Fourier transformation (Fourier transform infrared spectroscopy - FTIR). This method is quite old and is know since late 1960s, but at that time it was not used commercially because the computational power was not as good as today. This lead to the fact that Fourier-transform-based spectroscopic systems were rather large and expensive. Nevertheless, this is not a true anymore, the usage of such devices has become quite common.

The FTIR spectrometer works on entirely different principle, it in fact requires much simpler instrumentation, but far more complicated data processing. The basic difference is that unlike the dispersion instrument the FTIR spectrometer examines all the wavelengths coincidentally. Collimated light from a broadband infrared source passes into the optical system and impinges on a beam splitter. The beam splitter is made of a special material that transmits half of the radiation and reflects the other half. One half is reflected from the fixed mirror while the other half is reflected from the mirror that moves and then both beams impinge on a detector. As a result the path-length of the two beams is different (by optical path difference – OPD) so there will be destructive and constructive interference. The type of interferometer just described is known as Michelson interferometer (see Fig. 2.3). The resulting signal depends on the velocity of the moving mirror and contains a series of maxima and minima. It is called **interfero-**

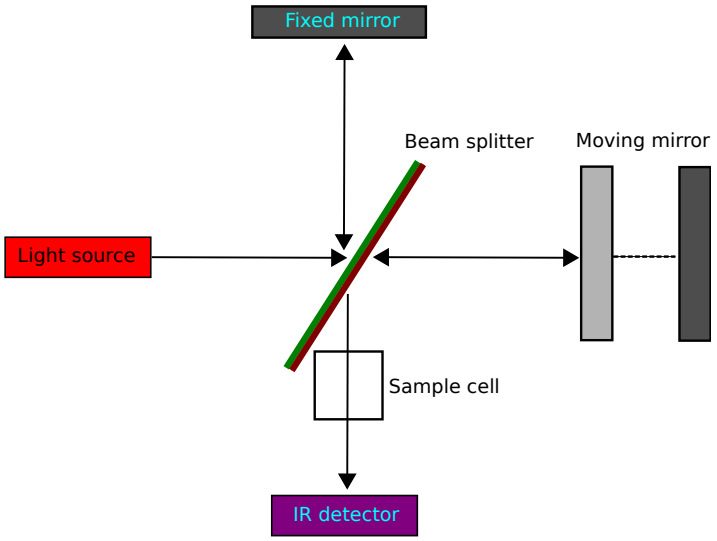


Figure 2.3: Michelson interferometer

**gram** which is a plot of relative intensity in dependence of relative mirror position. The actual absorption spectrum could be obtained be taking the Fourier transform of the interferogram. Compared to grating instruments FTIR spectrometer has following advantages:

1. Higher spectral resolution - In case of FTIR the resolution is simply given by the inverse value of the maximum achievable optical path difference. For example, FTIR spectrometer MIR 8025$^{\text{TM}}$has spectral resolution 0.02 nm at 700 nm. On the other hand with the dispersive model Cornerstone$^{\text{TM}}$ 260 1/4 m Grating Monochromator the maximum resolution of 0.15 nm could be achieved. These number might be also converted into inverse centimeters according to relation

$$\delta k = \frac{10^7 \delta\lambda}{\lambda^2}$$

where $\delta k$ means wavenumber resolution in cm$^{-1}$ and $\delta\lambda$ stands for wavelength resolution in nm, $\lambda$ for wavelength where the experiment is performed. In the light of this equation we find that 0.02 nm resolution corresponds to resolution of 0.5 cm$^{-1}$.

2. Better signal-to-noise ratio - The fact that FTIR spectrometer collects all the wavenumbers of light in one scan it shows that when spectra

are measured under identical conditions (same time of the experiment, same resolution, same source and detector) the signal-to-noise ration of FTIR spectrum will be greater then that of a dispersive spectrum by the factor of $\sqrt{N}$, where $N$ denotes number of scans. We speak about so called **Fellget advantage**. But this fact can be also seen from another angle since we do have a choice whether to get higher signal-to-noise ration for a given scan-time or shorter scan-time for a given resolution – detection of spectra in short time also enables time-resolved vibrational spectroscopy (especially Raman and resonance Raman).

3. Higher energy throughput - Resolution in dispersive spectrometers is obtained by the width of the slits which considerably decreases the energy throughput. FTIRs have no slits and so again their efficiency is better. This observation is known as **Jacquinot advantage**.

**Hole burning**

Spectral hole burning first of all relies on existence of inhomogeneous broadening and also on existence of some kind of molecular mechanism, which alters the homogeneous absorption spectrum upon absorption of light. High intensity spectrally narrow laser is needed as well. Hole burning enables to study biologically important molecular complexes that normally have low resolution at low temperatures. Molecules that are in resonance with laser frequency are due to photochemical or non-photochemical transformations removed from the absorption band. Consequently, hole is formed at that frequency (see Fig. 2.4). When photochemical changes occur, the excitation pulse causes molecules of the sample to interact with the environment and thus enabling their isomerization. Such a molecules with different structure (the photoproduct) contribute to absorption with a certain frequency shift. In the photochemical case the shift is equal or bigger than the inhomogeneous band width. In Fig. 2.4 recognize contribution of this effect as a dashed anti-hole at the very right of the spectrum. If there are non-photochemical changes the shift in frequencies of the photoproduct is smaller than inhomogeneous band width and according to the picture 2.4 the photoproduct manifests itself as an anti-hole on the of the absorption band. This is because in non-photochemical case the excitation pulse only causes slight conformational rearrangements in the molecule's environment

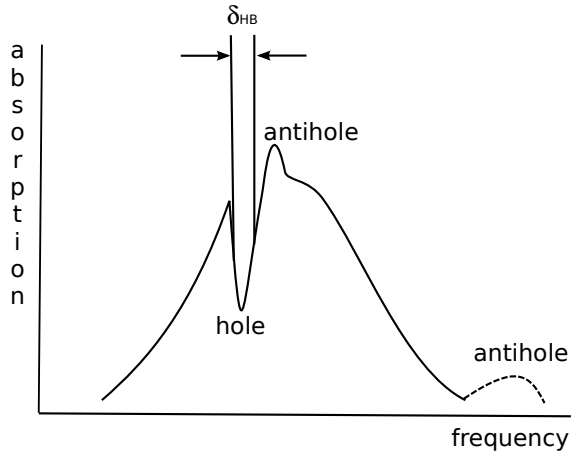


Figure 2.4: Depiction of spectral hole burned into an inhomogeneously broadened spectral line. Molecules whose transition frequencies lie in the spectral area of burning laser undergo photophysical or photochemical changes which cause them to absorb on different frequencies than before excitation. As a result anti-holes are observed. The width of a typical hole may be around 2 $cm^{-1}$.

(the effect of solvent shift[4]).

The hole width $\delta_{\mathrm{HB}}$ measured under proper experimental conditions determines the homogeneous width of the optical transition $\Gamma_{\mathrm{hom}}$ through the expression

$$\delta_{\mathrm{HB}} = 2\Gamma_{\mathrm{hom}} + \delta_{\mathrm{L}}$$

where $\delta_{\mathrm{L}}$ is the spectral width of the burning laser.

### 2.1.2 Time domain

**Fluorescence up-conversion**

Fluorescence up-conversion technique is used to record very short fluorescence lifetimes (femtoseconds). It is based on the nonlinear effect of sum frequency mixing in nonlinear optical crystal. Fluorescence up-conversion experiment is given by two phases. Firstly, the sample is illuminated by a strong excitation pumping pulse that induces fluorescence which is lead by mirrors to a nonlinear crystal. Secondly, the fluorescence light is overlapped

[4]For the definition of solvent shift see page 10.

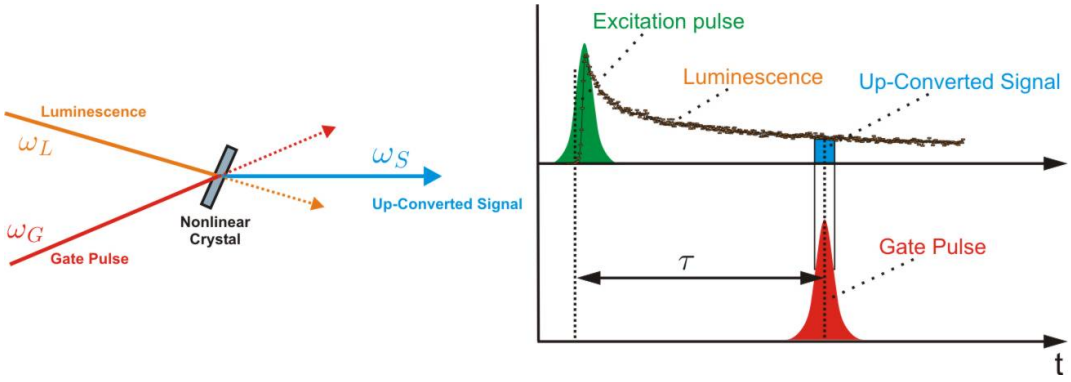


Figure 2.5: Fluorescence up-conversion principle. Fluorescence light and probing (gate) pulse form together in a nonlinear crystal signal with generally some new direction and new frequency. This signal is then measured and analyzed. By varying delay time between fluorescence and probe pulse lifetime of the excited state could be calculated.

by a probing gate pulse and together they generate up-converted nonlinear signal. Such a process is generally termed N-wave mixing a will be described later in this work in section 3.3. Sum frequency mixing only occurs as long as gate pulse and fluorescence are in the crystal at the same time and thus only the light of a very short time window can be seen (a time window roughly corresponding to the length of the gate pulse). Probing pulse is delayed with respect to the pumping pulse and by varying the delay time fluorescence decay can be monitored in the time regime which allows to observe the whole fluorescence time kinetics. Consequently, a relation between the fluorescence intensity and the delay time can be found so that the lifetime of the excited state could be deduced.

**Single photon counting**

Single photon detection technique – also called *Time Correlated Single Photon Counting* (TCSPC)– is another way in fluorescence spectroscopy to determine a lifetime of an excited state. But this time the resolution is not as high as in the case of fluorescence up-conversion. The maximum resolution goes not further than to a few picoseconds. It is thus not a true high resolution method but it definitely has some specific characteristics that are worth mentioning. The main advantage is that it can be used to measure lifetimes over approximately seven orders of magnitude, from

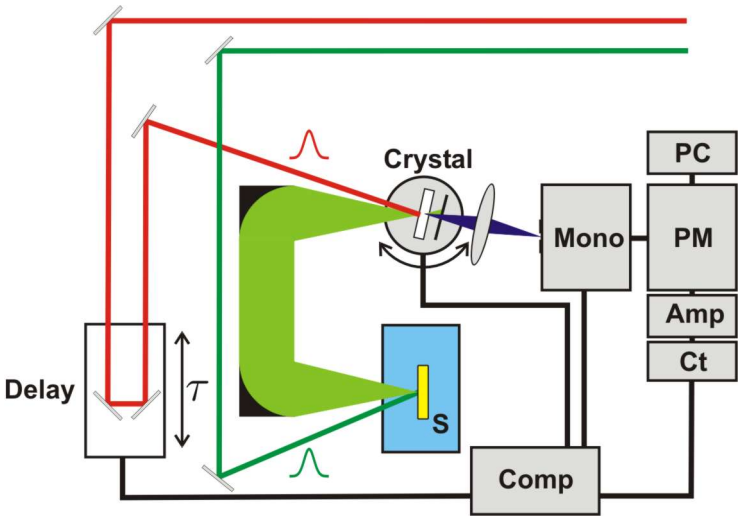


Figure 2.6: Fluorescence up-conversion experimental setup scheme. The excitation pulse (green in the picture) is through a system of mirrors aimed at the sample S and gives rise to fluorescence. Another (probing, red in the picture) pulse is delayed according to excitation pulse by time $\tau$ , arrives at a non-linear crystal and mixes there with a fluorescence signal. The frequency of the resulting non-linear signal is filtered by a monochromator (Mono), signal is then amplified by photomultiplier (PM) and registered in photon counter (PC).

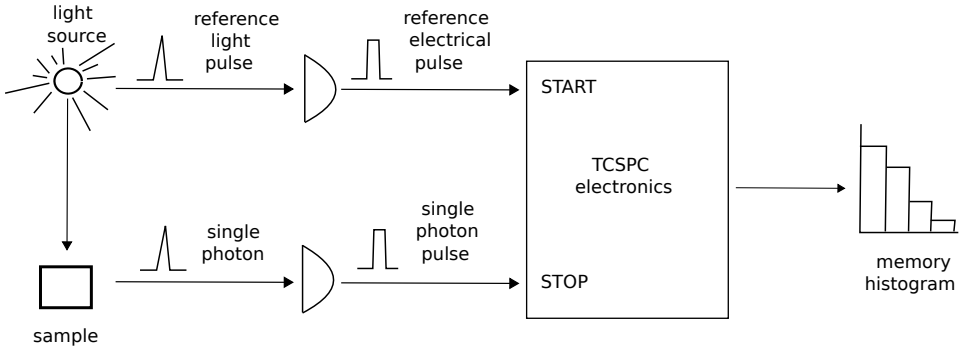


Figure 2.7: Schematic time correlated single photon counting experimental setup. The reference pulse sends a start signal to a counting mechanism, which is stopped after a photon arrives to the detector. Once the time between START and STOP is determined, the incident photon is registered in the corresponding time channel of the memory histogram.

picoseconds to tens of microseconds. The lower limit is given by the jitter of TCSPC electronics, while the upper limit arises from the time one can afford to acquire data with reasonable precision.

TCSPC is a statistical method and a high repetitive light source is needed to accumulate a sufficient number of photon events for a required statistical data precision. The main principle is to detect single photons and measure their arrivals to a detector in respect to a reference signal. It is schematically depicted in the Fig.2.7. We see a light source that sends a reference pulse into the detector. This pulse may be considered a START signal to an imaginary clock. Another pulse from the light source goes into the sample and induces fluorescence signal. Single photons can be detected with photodetectors having an intrinsic high gain. The majority of these detectors are photomultipliers. In a photomultiplier the photon is absorbed and causes an emission of electron (or photoelectric current) which is then amplified by the system of dynodes that are able to multiply the electric current as much as 100 million times. Also the single photon signal acts as a STOP signal to our imaginary clock. The time measured for one START-STOP sequence will be represented by an increase of a memory value in a histogram in which the single channels represent steps in time. The resulting histogram counts versus channels will represent the fluorescence intensity versus time. By fitting the intensity values in histogram with an appropriate function the excited state lifetime could be found.

## 2.2 Basics of the pump-probe technique

In the introduction on spectroscopy we talked about the measurement of absorbance as a function of frequency (or wavelength), which is a basic experiment allowing us to look into some of the system's characteristics. But if we want to find out more about the system, this method will not be sufficient. Let us say our intention is to learn about the kinetics of the system, about how system evolves in time. This is quite useful information, especially when we study photosynthetic light-harvesting systems, because the main interest of ours in this case is to see where the energy goes after the system absorbs light. A few decades ago we were not able to study photosynthetic systems' kinetics at that deep level as we are today. It was not until the invention of ultrafast lasers when this area became accessible and thus opened up new research opportunity and enabled investigation of such a photophysical and photochemical reactions in real time. The time scale on which the primary events of photosynthesis occur is in order of hundreds or even tens of femtoseconds. Effects of that kind belong to the fastest events in biology. Nowadays that the duration of laser pulses can sometimes go even as low as to the order of femtoseconds we have a really powerful weapon in our hands, because the resolution of our experiment is determined just with the laser pulse duration[5]. One of the experiments that make use of ultrafast lasers is called pump-probe technique. We will talk more about its various possible applications in the next section, here we will merely try to explain its fundamental principles.

Pump-probe experiment is a two-step process, in the first step a fraction of molecules is promoted to an electronically excited state by means of an excitation (or pump) pulse. This fraction typically ranges from tenths to tens of a percent. After that a weak probe pulse is sent through the system, usually with such a weak intensity that any multiphoton processes are avoided during probing. We may think of the probe pulse step as of a simple absorption experiment. But as you can easily imagine, the result of such absorption experiment will now vary with the time delay between the pump and probe pulses and because eventually all of the excited molecules will return back into the ground electronic state, after long enough time the results will not be any different from normal absorption spectra.

The scheme of the pump-probe experimental setup is depicted in the Fig.

[5]Depending on experimental setup the detector may also play a crucial role in final resolution

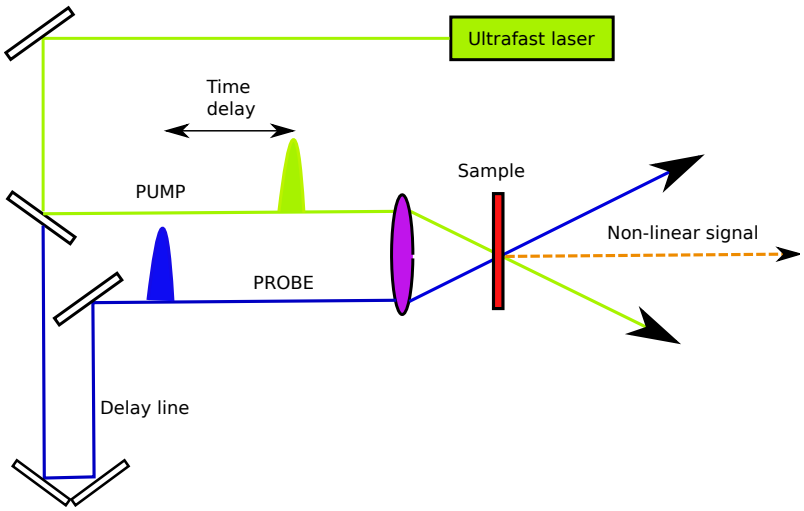


Figure 2.8: Pump probe experimental setup scheme

2.8 which may seem similar to that of fluorescence up-conversion. In fact, the only difference is that in pump-probe we measure absorption, while in fluorescence up-conversion we are interested in time evolution of fluorescence. The common feature is that both methods are based on non-linear effects.

Let us designate the delay time as $\tau$, and absorbance measured in the time $\tau$ as $A(\omega, \tau)$. Finally, let $A_0(\omega)$ stand for the absorbance of the sample without any pumping. Now we are able to define new quantity $\Delta A(\omega, \tau)$ as

$$\Delta A(\omega, \tau) = A(\omega, \tau) - A_0(\omega), \tag{2.11}$$

which we call **transient absorption spectrum** (or **pump-probe spectrum**[6]). $\Delta A(\omega, \tau)$ contains information on the dynamic processes that occur in the system, such as excited-state population, electron transfer processes, isomerization, and intersystem crossing. Generally, we can divide transient absorption spectrum into a number of contributions from various processes. Here is a list of these contributions:

1. The first contribution is by *ground-state bleach* (red line in the figure 2.9). Through the action of the pump pulse promoting some fraction of molecules to their excited states, absorption from ground state decreases because of the lower number of molecules remaining in the

[6] We will use these two term interchangeably.

ground state. Hence, the ground-state absorption becomes less than that of the non-excited sample. Consequently, in transient absorption spectrum a negative signal is obtained in the frequency region of ground state absorption.

2. Another contribution to $\Delta A(\omega, \tau)$ comes from *stimulated emission* (green line in figure 2.9). During this process a photon from the pump pulse passes through the sample and induces another photon emission by forcing a molecule at the excited state to get back to the ground state. After that both of these photons travel in the same direction and both are registered in a detector. Such a process results in an increase of the detected signal, corresponding to a negative $\Delta A(\omega, \tau)$ signal. Considering that Einstein coefficients for absorption and stimulated emission are identical the two of these so far mentioned contributions will have the same spectral profile, only with stimulated emission curve slightly shifted to the lower frequencies (Stokes shift). It happens though that the Stokes shift is too small that both lines are indistinguishable from each other.

3. The third contribution is provided by *excited-state absorption* (blue line in figure 2.9). In certain frequency regions excitation of a sample may be followed by transitions to higher excited states. This results in observing a positive signal in the transient spectrum.

4. The fourth possible contribution to the $\Delta A(\omega, \tau)$ is given by what we call *product absorption*. Sometimes in photobiological system there exist a possibility for excited molecules to undergo certain reactions resulting in a long-lived molecular state, such as triplet state, charge-separated state or isomerized state. Product absorption appears in the transient spectrum as positive signal.

For a complete picture we would like to add that whenever there is an absorption or spontaneous emission process caused by the probe pulse, the population of the excited state does not change significantly. This assumption could be made because of the relative weakness of the probe pulse in comparison to the pump.

Lastly, we would like to present a very simple illustration of the pump-probe experiment, it is shown in the figure 2.10. It consists of a set of five spectra and three different peaks at identical positions for all of the five lines, while each line corresponds to some particular delay time $t$ between

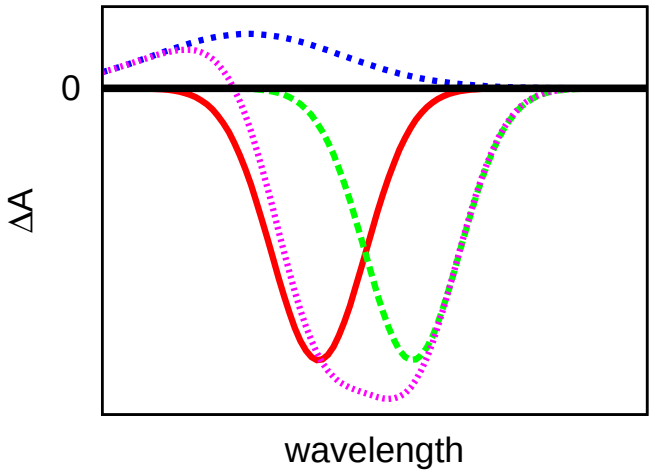


Figure 2.9: Schematic depiction of pump-probe absorption spectroscopy principle. Red line - ground state bleach, green line - stimulated emission, blue line - excited-state absorption, pink line - sum of these contributions

pump and probe pulses. The experiment has been performed on the solution of $[H_2TPPS_4]^{4-}$ dissolved in the buffer of pH = 8. However, it is not our intention to go that far in details here as our main goal is mostly to stress the essential characteristics of the spectrum. The sample has been excited with the help of laser operating at the wavelength of 420 nm and after that it has been probed throughout the range from 350 - 750 nm. At the wavelength of 422 nm we can see the peak that has a descending tendency in time. It could be easily verified by normal absorption experiment that this peak could be matched to ground state bleach (because the absorption occurs at the same wavelength). The maximal size of the peak at the time $t = 0$ is interpreted as a maximal amount of molecules in excited states. As the experiment progresses in time this amount becomes gradually smaller and smaller and at $t = 10\,000\,\mathrm{ns}$ the number of excited molecules reaches near zero which is in agreement with the vanishing $\Delta A$ signal at this time. The other peak at $\lambda = 460\,\mathrm{nm}$ reflects the origin of the new electronic transition as is indicated by the fact that this peak is of opposite sign in comparison to the ground state bleach. In other words the absorption has increased in this region after the impingement of the excitation pulse. In this case the new electronic transition emerged between the ground and first excited triplet states. The last part of our spectrum is the wide band in the

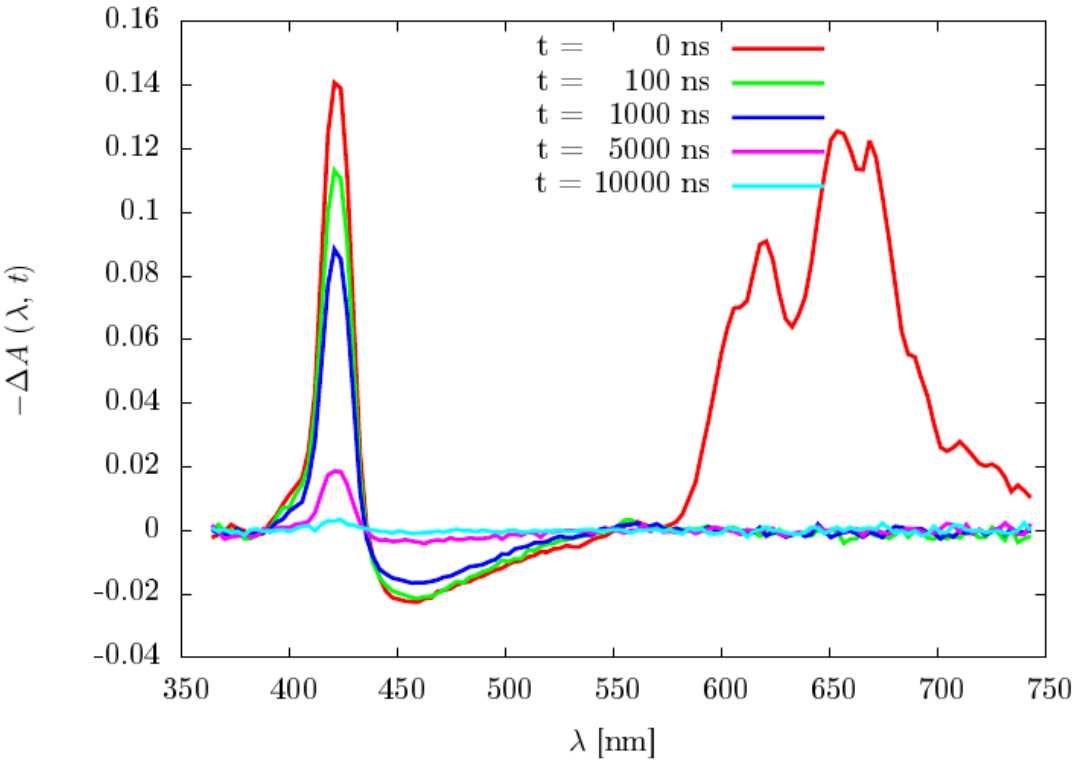


Figure 2.10: Example of a simple pump-probe experiment

red spectral region. It differs from the former two in its duration, which does not get over the tenths of nanoseconds. That is why it could be considered a manifestation of fast fluorescence. It is quite common to approximate the changes in transient absorption spectra by a single exponential function in the form

$$\Delta A(\omega, \tau) = \Delta A(\omega, 0) \exp\left(-\frac{\tau}{\tilde{\tau}}\right) \tag{2.12}$$

$\tilde{\tau}$ denoting the lifetime of the excited state at frequency $\omega$. Making use of this relation both lifetime of first excited singlet state and first excited triplet state was obtained.

This experiment is also a good demonstration of other two interesting things. Firstly, it shows how strong the applicability of this method is. It practically ranges from microseconds (which is the typical order of triplet state's lifetime – measured in the experiment) to the order of magnitude $10^{-15}$ s (typical order of energy transfer rate in photosynthetic systems). As we already mentioned above, the final resolution is mainly given by the duration of both the pump and the probe pulses. Secondly, we would like to mention one little technicality regarding the presented graphs in 2.9 and 2.10. While the former one is showed in a form where ground state bleach

gives negative contribution the letter one depicts the same contribution in the positive half-plane. Both of these alternatives satisfy definition (2.11) and both of these alternatives could be seen in articles and may thus cause a little confusion in the reader. However, recently there has been a prevailing tendency to stick to the alternative from Fig. 2.9.

## 2.3 Applications of the pump-probe technique

If we wanted to list all possible applications of the pump probe technique, it would surely be enough for a considerably large publication. Its usage in molecular aggregate dynamics studies and biological systems research is extensively wide. Especially when talking about scientific efforts on the field of discovering function of photosynthetic systems it proved to be very valuable. Despite the fact that nowadays we have at our disposal a great number of other spectroscopic methods, it still occupies a unique and respected position in the field. The common feature of all pump probe experiments is the determination of temporal changes that occur under properly chosen lighting conditions. This means that in principle every pump probe experiment has the same fundamental properties and in fact the only thing remaining is to tell what exactly is changing, why is it changing and how. In the next few lines we would like to provide some interesting (and in some cases maybe even unsuspected) examples where pump probe showed really helpful. After that we decided to include two short presentations with more complete explanation of the investigated problem and interpretation of the obtained spectra.

There is no need do debate that devices such as light emitting diodes (LED) are now an indisputable part of humans life, and we could definitely find more that one material applicable to their construction. We may for instance mention organic light emitting diodes (OLED), or polymer light emitting diodes (PLED). Both these devices are well suited for an experimental treatment on the basis of pump probe. That is because we know that a key process in molecular and organic electronics is *triplet energy transfer*. What we talk about here is an energy migration along a selected molecular structure that usually occurs in two different modes. The first one is single step tunneling and the second is know as *multistep hopping*. And that is exactly the situation where we are able to study the energy transitions

by implementation of the high resolution spectroscopic technique[7] and evaluation of transient absorption data which provides us with a map of the system's dynamics. This way we can find a crossover between the above mentioned modes and hopefully use it for our advantage in the pursuit for better understanding and designing energy transfer pathways in the LED devices. However, these are not the only structures where triplet energy transfer may be found. This rapid and efficient transport of energy and charge over tens to hundreds of nanometers is also crucial for thin film transistors, organic photovoltaic or long-distance energy transfer in proteins. For more detailed investigation I refer to [10].

Another very nice example are studies performed with an intention to put some light into mechanism of repair processes in DNA molecules. Following information published in Ref. [5] we build our discussions upon the fact that so called (6-4) photoproduct has detrimental effects on the replication and transcription and may result in mutations and even cell death. (6-4) photoproduct usually arises from actions of ultraviolet radiation and the mechanism of its repair is still in the stage of poor understanding. Reactions that underlie the repair are rather complex, but still with the help of ultrafast spectroscopy some new insights may be revealed.

The other example comes from the field of capturing solar energy with semiconductor solar cells which typically absorb photons with energies above the semiconductor bandgap. The additional energy of these photons is converted into so called hot charge carries (electrons and holes) that quickly cool by sequential emission of phonons (this process standardly occurs on the timescale of 1 ps). The maximum efficiency of a semiconductor solar cell is then determined by our technological ability to extract these hot carrier and produce electrical current. Today it is not more than approximately 30%. But there is a potential route to construct solar cell with higher efficiency, theoretically to as high as 66%, with help of semiconductor nanocrystals, or quantum dots, which in principle enable extraction of hot carriers before they cool. Ultrafast absorption spectroscopy enables us to successfully study electron transfer in these structures and hopefully to make some new progress. As a reference to this topic we would like to refer you to [9] where these problems are dealt with quite thoroughly. Authors show here that electron transfer from the higher excited states of a colloidal semiconductor nanocrystal (PbSe) to a common electron acceptor ($TiO_2$) is

[7] Temporal resolution in order of few hundreds of femtoseconds is required to get some results.

indeed possible. And again, pump-probe experimental technique has been used.

Let us dedicate the last paragraph to the application in x-ray powder diffraction. Our goal in these kinds of detection is to find a charge density map of a studied material, which can be derived from the diffraction pattern. Standard methods used for this purpose are x-ray diffraction from polycrystalline samples or the Debye-Sherer diffraction technique. Naturally, both of these methods lead in principle to the phase problem, the critical point of x-ray diffraction. Reliable methods for solving this problem originated long time ago and many information about crystallic structures have been revealed. But there is a remarkable extension to these methods and that is namely a study of atomic motions in femtosecond time domain[8]. This allows for mapping molecular structure generated by basic chemical and biological processes and for deriving transient electronics charge density maps. In other words the sample is electronically excited via fast femtosecond pump pulse at optical frequency and the resulting structural dynamics is probed by hard x-ray (also femtosecond) pulse. This way a direct evidence of the ultrafast nature of the induced dynamics has been obtained for chosen samples (see [3]).

After this short review of transient absorption spectroscopy applications we decided to discuss two recent experiments more thoroughly in order to bring at least a little more real image of the main characteristic features about this strong and versatile method. The goal is not to provide any specialties as far as the applied experimental setup or exploited computational methods of data interpretation are concerned. Respecting the intended extent and purpose of this thesis it is far enough for us to pay a brief but careful attention to the resulting spectra and their proper interpretation. After all, the capability of pregnant reading of the output plays often one of the most important roles in spectroscopy.

### 2.3.1 Illustrative example no. 1

In recent time there have been many attempts not only to fully understand but also to control the motion on a molecular scale. This aim of modern science is nicely demonstrated in Ref. [8] where authors decided to reveal molecular operations of rotaxane complexes where a macrocycle shuttles be-

[8]Pump-probe experimental scheme used in [3] provided experimentators with time resolution about 100 fs and spatial resolution around 30 pm.

tween two stations along an axle[9]. We can envision rotaxanes as macrocyclic rings trapped onto a linear unit by two bulky substituents (stoppers). Approximate description of the structure of the particular rotaxane complex studied in the cited experiment is depicted in the Fig. 2.11. It consists of two stations (succin amide station – succ, green in the figure – and naphtalimide station – ni, grey on the figure), one macrocycle (blue) and a hydrocarbon chain, whereas in neutral molecule the macrocycle is predominantly hydrogenbonded to the succ station. However, if an excitation light pulse of a suitable wavelength is used the macrocycle may loose its affinity to succ station and start moving along the axle to the other station. Here, this really happens. After the rotaxane is excited it undergoes fast intersystem crossing into the triplet state and then the ni station is reduced from an external donor to form a radical anion (process of charging in 2.11). Indeed, the affinity of the macrocycle to this anion is greater than to the succ station. Therefore the macrocycle quickly makes its way to the other side of the molecule and stays there until after the charge recombination of the ni anion takes place.

In order to monitor molecular machine motion with sufficient enough precision the experimental requirements are quite strong. Primarily, both structural and temporal resolutions have to be reasonably high. Of course, this goal could be easily achieved by employing the pump probe method[10] where time resolution is determined by the pulse duration which could by less than hundreds of femtoseconds. In this particular experiment there was no need to go as far as into the femtosecond scale, because the main dynamics of the molecular machine happen mostly at the order of nanoseconds, hence a nanosecond pump pulse was applied. On the other hand, much shorter probe pulse (100 fs) provided the experimentators with the spectral bandwidth necessary to probe the entire rotaxane absorption spectrum in one laser pulse. The results of the measurements are shown in Fig. 2.12. The difference absorption spectrum has been scanned at the interval between 1580 and 1720 $cm^{-1}$ and for ten different delay times between pump and probe pulses (listed in the Figure). We would like to remind that our picture does not reproduct the original data, but only copies the most important patterns.

Altogether, there are seven evident peaks in the spectrum and each peak

[9]Such a task is quite a challenge as some of the standard macroscopic concepts often loose meaning on microscopic level.

[10]In this case time-resolved vibrational pump-probe has been adopted.

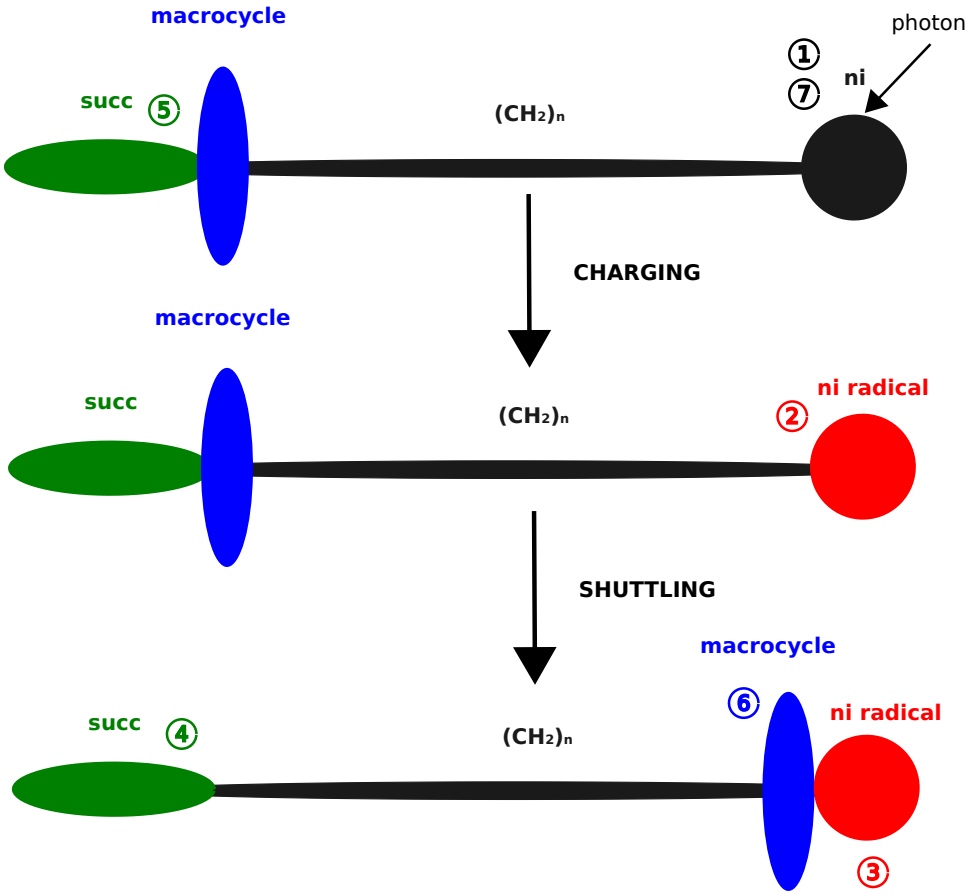


Figure 2.11: Structure of the rotaxane molecular machine composed of two stations (succ and ni) and one macrocycle. After excitation with the pump light pulse rotaxane undergoes fast intersystem crossing relaxation into the triplet state where is reduced by an external donor to the radical form. In this form the radicalized ni station has greater affinity to the macrocycle than the succ station and the macrocycle starts to shuttle along an axle between the stations. Using the pump-probe technique both rate constant of the shuttling and binding energy of the macrocycle could be determined. The numbers in the picture correspond to some prominent CO bonds and their meaning is following: 1+7) ni station resides in its normal form 2) ni in radical form 3) ni with the macrocycle bonded 4) alone succ station (without the macrocycle) 5) succ with the macrocycle 6) macrocycle arriving to ni radical

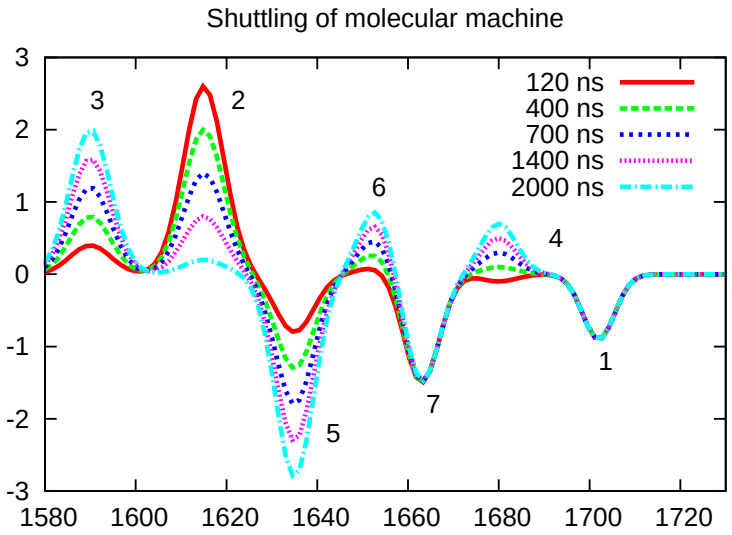


Figure 2.12: Reconstruction of transient absorption spectrum of the rotaxane molecular machine in the spectral region from 1580 to 1720 $cm^{-1}$ registered with help of vibrational pump-probe. The numbered spectral peaks correspond to the CO bonds of rotaxane complex as shown in figure 2.11.

corresponds to some characteristic CO bond in the rotaxane structure. The proper assignment of the peaks to the corresponding bonds is again apparent from the figure 2.11. Usually, steady-state absorption spectra could be used to find the position of each particular peak in the spectrum. Here, spectra of the initial, charged and final states had to be studied first. For example, let us have a look at the peaks 1 and 7 which are assigned to the uncharged ni station. It is obvious that in the whole time range there has been no evolution in the number of uncharged ni in the sample. That is because the charging event has already taken place in the first phase of the experiment, i.e. at times under 120 ns. On the contrary there is clearly something happening with the peak number 2. At the beginning it reaches the highest values of differential absorption and as the experiment proceeds it gradually loses its intensity. This effect might be interpreted as the decrease in the number of the radicalized ni stations which in the process of shuttling are substituted by the (ni+macrocycle) complex that absorbs at slightly different frequency. This fact is also confirmed by the increase of intensity in the spectral region corresponding to the number 3 which describes the arrival of the macrocycle to the ni side of the rotaxane molecule. As for the number 4 it again monitors the shuttling process, but now in terms of the increase of the number of the alone succ stations (without the macrocycle bonded). This is how an increase in absorption of the peak no. 4 is explained. Similarly we could describe the meaning of the remaining peaks and its correspondence to the CO bonds in rotaxane complex.

To draw a conclusion we found out that the rotaxane undergoes a certain dynamics that is connected with the shuttling process of the macrocycle. From the spectrum 2.12 we are able to obtain the rate constants for the observed events (in the simplest way using relation similar to 2.12) and thus the shuttling time could be determined. But that is not all, these findings could be expanded and other important information about the system may be revealed. For example, with the help of Eyring equation

$$k(T) = \frac{k_B T}{h} \exp\left(-\frac{\Delta G}{RT}\right), \tag{2.13}$$

where $k_B$ stands for Boltzmann constant, $h$ for Planck constant, $R$ for gas constant, $T$ for temperature and $\Delta G$ for the Gibbs free energy, it is possible quantify the energy barrier that the macrocycle must overcome to escape from the succ station. The only thing we have to do is to calculate the temperature dependence of the rate constant $k$.

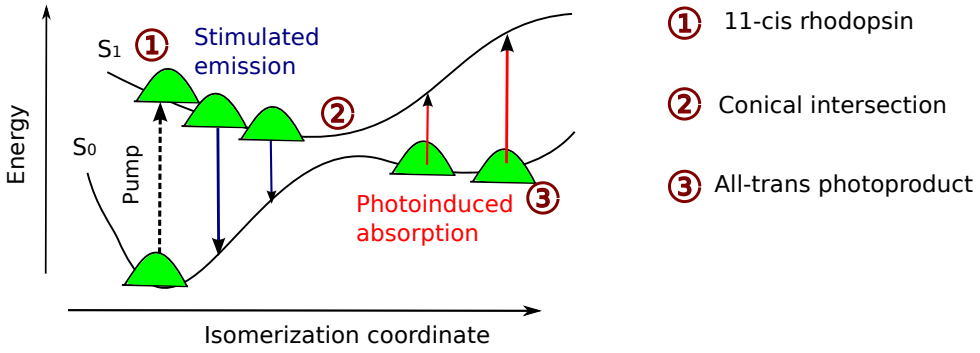


Figure 2.13: A sketch of isomerization potential energy surfaces of rhodopsin *a* and the corresponding structural changes rhodopsin undergoes as it progresses along the isomerization coordinate. Roughly speaking, during the first 80 fs stimulated emission signal of decreasing frequency is observed while after that the stimulated emission vanishes and an absorption shifting into the blue region of the spectrum arises.

### 2.3.2 Illustrative example no. 2

The next illustration of pump-probe experimental method regards dynamical processes in vision (according to Ref. [6]). The conversion of 11-cis retinal chromophore to its all-trans form in rhodopsin has been for a long time considered the primary photochemical event in vision. Rhodopsin is a uniquely reactive pigment and the very first reactions that take place during the perception of light usually occur within the mere 200 fs which suggests an unusually fast energy redistribution. It is believed that this remarkably fast reactivity is caused by a conical intersection between the potential energy surfaces of the ground and excited electronic states of rhodopsin. For the purpose of registration of such events ultrafast optical spectroscopy with a time resolution less than 20 fs has been used and the spectrum has been registered from the middle visible to the near infrared. The main goal should be here to present a plausible evidence for the existence and importance of conical intersections in visual photochemistry. That meas to track the events along the rhodopsin isomerization coordinate and put a propriate interpretation.

The photoisomerization was initiated with a 10-fs 500-nm pump pulse that brought rhodopsin into the excited state and the duration of probe was no longer than 15 fs. It is important to emphasize that these two facts are the key to observing the transitions between the ground and excited states. The

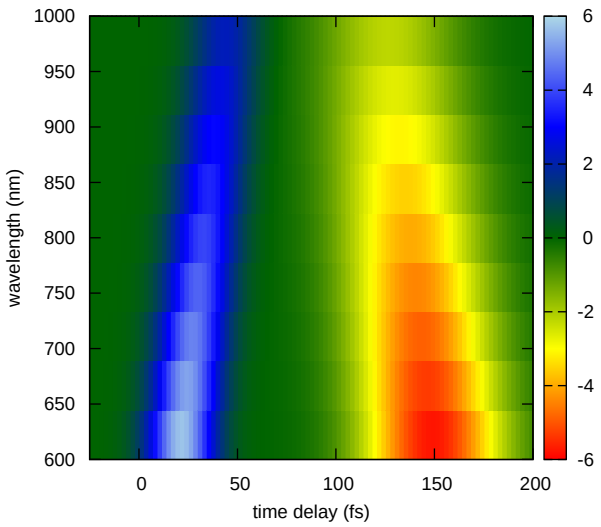


Figure 2.14: Two dimensional pump-probe spectrum showing dynamics through the rhodopsin conical intersection.

evolution of the rhodopsin complex could be understood with the help of Fig. 2.13 where the approximate shape of both ground and excited state potential energy surfaces along the isomerization coordinate is plotted. When the incident light gets through the sample and the first excited state is populated the rhodopsin transient absorption spectrum exhibits a positive signal which is assigned to stimulated emission from the excited state. This signal rapidly shifts to the red part of spectrum and at the same time looses its intensity. Within approximately 80 fs it disappears which suggests rhodopsin to arrive at the conical intersection of both potential energy surfaces. Right after that there originates a negative absorption signal that initially appears at 1000 nm (the same wavelength where stimulated emission have vanished) and gradually shifts to the blue and increases in intensity.

This course of events is mapped in Fig. 2.14 which shows a two-dimensional transient absorption spectrum. The blue part represents spontaneous emission and the yellow part stands for absorption. As in the previous example, we did not use the original date to make this plot, we only tried to capture the characteristic behavior.

Again we saw how effective the pump-probe method might be. We have intentionally chosen two examples from two relatively different fields to prove its rather considerable universality. Besides that we have seen that depending on the purpose of the experiment the data can be presented in both one dimensional and two dimensional way.

## 2.4 Introduction to 2D spectroscopy

Two-dimensional spectroscopy is a revolutionary spectroscopic method that provides new and interesting insights into understanding of complex molecular systems. It contains a great amount of information that could be used to study not only function of the molecules but it can also indirectly reveal some structural features. It could be used to study population coherence dynamics of excited molecules as well as to reveal inhomogeneous structures of lineshapes.

2D spectroscopy could be performed in both visible and infrared region of the spectrum and with femtosecond resolution. From practical point of view its experimental realization corresponds to that of 4-wave mixing experiment which we describe in great detail in the next chapter. The resulting two-dimensional spectrum of a common molecular system usually shows many peaks that overlap and are hard to separate. In an ideal spectrum we would be able to distinguish diagonal and off-diagonal peaks (cross-peaks). While the diagonal peaks correspond to linear spectrum, the cross-peaks show coupling between electronic excitations. The oscillations of cross-peaks reveal electronic coherences and changes in their intensity is often the sign of relaxation processes. Finally, two-dimensional spectrum includes information about absorption spectrum, stimulated emission or excited state absorption (ESA).

As for the formal definition of the two-dimensional spectrum we decided to postpone it to the next chapter since there is no easy and transparent way to do that without having the whole non-linear theory built-up first.

# Chapter 3

# Theory of nonlinear response functions

In this chapter we are going to devote ourselves to description of the theory behind measuring spectroscopic signal. Especially we are going to set forward a theoretical method of interpreting a pump-probe experiment. This will be our main goal here, but many of the facts explained will relate to such general rules that they could very well find another usage in various fields of spectroscopy.

Our first step will be to remind ourselves of the Maxwell equations of electromagnetic field, which is the standard set of four equation for the fields $\vec{E}$ - electric field, $\vec{B}$ - magnetic field, $\vec{D}$ - electric displacement field and $\vec{H}$ - magnetic displacement field. The four fields are not independent of each other. For $\vec{D}$ we have

$$\vec{D} = \varepsilon_0 \vec{E} + \vec{P} \tag{3.1}$$

and similarly for $\vec{H}$

$$\vec{H} = \frac{\vec{B}}{\mu_0} - \vec{M}, \tag{3.2}$$

where $\vec{P}$ stands for polarization and $\vec{M}$ for magnetization of a material, $\varepsilon_0$ for vacuum permittivity, $\mu_0$ for permeability of a free space. However, we do not assume our materials to be magnetic and so we neglect the second term in equation (3.2) and consider $\vec{H} = \vec{B}$. On the other hand the polarization from Eq. (3.1) will become one of the most important quantities for us. It usually comprises two parts, one that refers to the existence of permanent dipoles in the system and one that reflects the formation of transition dipole moments in molecules which is only possible if the sample has

been exposed to some kind of electromagnetic field first[1]. Under its effects some molecules undergo a process of excitation that changes the distribution of charge density, making it inhomogeneous and creating thus a temporal dipole. As soon as the deexcitation occurs transition dipole vanishes. From these two possible forms of polarization we calculate only with the second one, leaving out materials with permanent dipoles. We also do not consider neither any electrical charges, nor any electric currents present. Omitting the corresponding terms form Maxwell equations we can write these in the form

$$\nabla \cdot \vec{B}(\vec{r},t) = 0, \tag{3.3}$$

$$\nabla \cdot \vec{D}(\vec{r},t) = 0, \tag{3.4}$$

$$\nabla \times \vec{B}(\vec{r},t) = \mu_0 \frac{\partial \vec{D}(\vec{r},t)}{\partial t}, \tag{3.5}$$

$$\nabla \times \vec{E}(\vec{r},t) = -\frac{\partial \vec{B}(\vec{r},t)}{\partial t}. \tag{3.6}$$

We will not make any significant use of the first two equations. Eq. (3.3) only reminds us of the fundamental property of magnetic field, that $\vec{B}$ is purely transversal. Eq. (3.4) shows that in neutral systems $\vec{D}$ is a transversal field as well. But also the incoming field $\vec{E}$ will be considered not to contain any longitudinal component, because the main role in all of our thought experiments will be played by laser beams and pulses that propagate through space in the form of electromagnetic waves. Consequently, polarization $\vec{P}$ will not have any other chance, but to stay in transversal form either. Now we can finally turn our attention to the latter two equations from which we are able to derive a differential equation that formally puts in connection electric field and polarization. That equation reads as

$$\nabla \times \nabla \times \vec{E}(\vec{r},t) + \frac{1}{c^2}\frac{\partial^2}{\partial t^2}\vec{E}(\vec{r},t) = -\mu_0 \frac{\partial^2}{\partial t^2}\vec{P}(\vec{r},t), \tag{3.7}$$

where we made use of the identity

$$\varepsilon_0 \mu_0 = \frac{1}{c^2}.$$

[1]Not any field of course, it has to contain frequencies that lay in the absorption band of our sample.

## 3.1 What is a response function

Before we expand our thoughts in more detail let us formulate the key task. Let us have a short look at the figure 3.1. In any spectroscopic experiment we deal with either light or some other kind of radiation. In order to get some information and find out what is happening in a sample we use a light beam and send it in. In our picture this is represented by $E_{in}$ - an incoming electric field. As the field travels through the sample it interacts with molecules and induces polarization $P$ which then back interacts with the field and makes it change. $E_{out}$ - an outgoing electric field - is affected by the polarization and carries information about the system, it can be detected and analyzed. The more we know about the outgoing signal, the more we can say about the system. And the key for this purpose is just the polarization which is responsible for all possible changes in electric field we measure. At the same time polarization could be easily interpreted from microscopic point of view and act as a connection between detected signal and dynamics deep inside the system. Therefore, our aim is to follow this scenario:

1. Find a link between $E_{in}$ and $P$ (see this section)
2. Find a link between $E_{out}$ and $P$ (see section 3.3)
3. Find a link between macroscopic $P$ and dynamics on microscopic level (see section 3.4)

As the first possible approximation, let us assume that the polarization $\vec{P}(\vec{r},t)$ depends on the incoming electric field $\vec{E}(\vec{r},t)$ linearly. Most generally this can be expressed as

$$\vec{P}(\vec{r},t) = \int_{-\infty}^{+\infty} \mathrm{d}\vec{r'} \int_{0}^{t} \mathrm{d}t' \bar{S}(\vec{r}-\vec{r'},t-t')\vec{E}(\vec{r'},t'), \tag{3.8}$$

where $\bar{S}(\vec{r}-\vec{r'},t-t')$ is the **linear response function** or the **first order response function**[2]. This definition will turn out to be very useful and of great benefit to us. For example, the whole theory of linear absorption can be expressed in the language of response functions. In our next section we

[2]Since there are quite often used temporally narrow laser pulses in spectroscopy we are allowed to take the expression of the electric field in terms of delta function which says that the laser pulse of a certain magnitude acts in a certain time.

$$\vec{E}(\vec{r},t) = \vec{E_0}\delta(t-T).$$

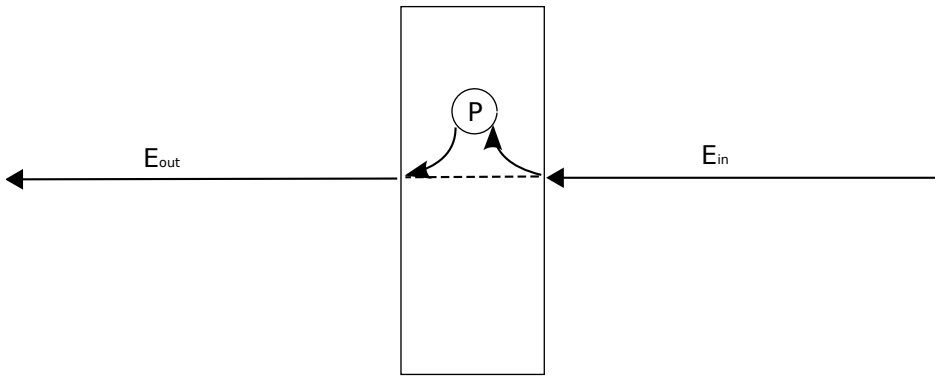


Figure 3.1: General process of light-matter interaction. Respective arrows may be interpreted as follows: 1) $E_{in}$ enters the sample and creates polarization $P$. 2) Polarization affects incoming field. 3) Affected field leaves the sample an is registered by a detector.

are going to demonstrate how linear response function helps us to calculate absorption coefficient of a medium.

## 3.2 Linear absorption

Let our medium be a simple isotropic sample and let the incoming field be in the form of a plane wave. We also choose the direction of its propagation to be along one of the axes of the Cartesian coordinate system, let say $z$. Electric field then reads

$$\vec{E}(\vec{r},t) = \vec{E}(z,t) = \vec{E}_0 \exp(ikz - i\omega t). \tag{3.9}$$

Now by substituting definition (3.8) into the original equation (3.7) we get

$$\nabla \times \nabla \times \vec{E}(\vec{r},t) + \frac{1}{c^2}\frac{\partial^2}{\partial t^2}\int_{-\infty}^{+\infty} \mathrm{d}\vec{r'} \int_0^t \mathrm{d}t' \bar{\varepsilon}(\vec{r} - \vec{r'}, t - t')\vec{E}(\vec{r'}, t') = 0, \tag{3.10}$$

Also the response function could be considered localized in a concrete position given by the vector $\vec{R}$ and again we can describe this property with a delta function $\delta(\vec{r} - \vec{R})$. In the view of this choice there emerges a simple interpretation for the linear response function according to which the polarization

$$\vec{P}(\vec{r},t) = \vec{E}_0 \bar{S}(\vec{r} - \vec{R}, t - T)$$

is nothing but a response to the field that acted at $\vec{R}$ at a time $T$ before now.

where by $\bar{\varepsilon}(\vec{r}-\vec{r'},t-t')$ we denoted the **dielectric function** in space and time domain defined as

$$\bar{\varepsilon}(\vec{r},t)=\delta(\vec{r})\delta(t)+\frac{1}{\varepsilon_0}\bar{S}(\vec{r},t). \tag{3.11}$$

Having in mind condition (3.9) and by some formal rearrangements in the expression of the second term in equation (3.10) we get to the conclusion that dielectric function may as well be formulated in the wavevector and frequency domain

$$\bar{\varepsilon}(\vec{k},\omega)\vec{E}(\vec{r},t)=\int_{-\infty}^{+\infty}\mathrm{d}\vec{r'}\int_0^t \mathrm{d}t'\bar{\varepsilon}(\vec{r}-\vec{r'},t-t')\vec{E}(\vec{r'},t') \tag{3.12}$$

or shortly (reminding of the definition of Fourier transformation)

$$\bar{\varepsilon}(\vec{k},\omega)=\int_{-\infty}^{+\infty}\mathrm{d}\vec{r}\int_0^t \mathrm{d}t\bar{\varepsilon}(\vec{r},t)\exp(i\vec{k}\vec{r}-i\omega t) \tag{3.13}$$

Straightforward application of this procedure to the equation for the dielectric function takes us to the well-know relation

$$\bar{\varepsilon}(\vec{k},\omega)=1+\bar{\chi}(\vec{k},\omega) \tag{3.14}$$

between $\bar{\varepsilon}(\vec{k},\omega)$ and $\bar{\chi}(\vec{k},\omega)$ which is the **linear susceptibility**. As you can see we introduced this fundamental quantity as the Fourier transform (FT) of the first order response function.

$$\varepsilon_0\bar{\chi}(\vec{r},t)=\mathrm{FT}(\bar{\mathrm{S}}) \tag{3.15}$$

This means that every relation that involves susceptibility is also directly related to the theory presented in this work. But before we move on to the main goal of this section – finding the dependence of linear absorption coefficient on $\bar{\chi}$ – we have to clear up one other thing. Again we talk about familiar relation

$$\bar{\varepsilon}(\vec{k},\omega)=\frac{k^2c^2}{\omega^2} \tag{3.16}$$

which is easy to find because the second time derivative in equation (3.10) now after transferring the dielectric function into wavevector and frequency domain touches only the electric field $\vec{E}(\vec{r},t)$ and thus it only gives factor

$\omega^2$. And as for the first term the double vector product of the nabla operator with the electric field could be rewritten according to the vector identity

$$\nabla \times \nabla \times \vec{F} = \nabla\nabla \cdot \vec{F} - \nabla^2\vec{F}, \tag{3.17}$$

which gets even simpler when we recall that the field we treat has no longitudinal component and thus has zero divergence. In the case of (3.9) employing Laplace operator is the same as taking the second partial derivative of $z$. Therefore the factor $k^2$.

Thanks to the isotropic nature of our sample we need not consider $\bar{\varepsilon}(\vec{k},\omega)$ a tensor. So from now on we take the liberty of giving up the bar symbol and start to consider dielectric function a scalar. But we know it is still a complex function and we can write for its square root

$$\sqrt{\varepsilon(\vec{k},\omega)} = n(\omega) + i\kappa(\omega) = \frac{kc}{\omega} \tag{3.18}$$

Here we have $n(\omega)$ – the **index of refraction** – and $\kappa(\omega)$ – the **extinction coefficient**. As the next step we express wavevector $k$ and use it in the definition of the plane wave (3.9). This yields

$$\vec{E}(z,t) = \vec{E}_0 \exp(ik'z - i\omega t - \frac{1}{2}\kappa_a(\omega)z), \tag{3.19}$$

where renormalized wavevector $k'$ and **absorption coefficient** $\kappa_a(\omega)$ are

$$k' = \frac{\omega n(\omega)}{c}, \tag{3.20}$$

$$\kappa_a(\omega) = \frac{2\omega\kappa(\omega)}{c}. \tag{3.21}$$

In this notation the field intensity is

$$I(z) \approx |\vec{E}(z,t)|^2 = I_0 \exp(-\kappa_a(\omega)z) \tag{3.22}$$

Finally we are able to relate absorption coefficient and linear response function. We take the square root of equation (3.14) and divide the susceptibility into its real and imaginary parts, $\mathrm{Re}\chi(\omega) = \chi'(\omega)$, $\mathrm{Im}\chi(\omega) = \chi''(\omega)$

$$\sqrt{\varepsilon(\omega)} = \sqrt{1 + \chi'(\omega) + i\chi''(\omega)} = n(\omega) + i\kappa(\omega). \tag{3.23}$$

Taking this expression to the power of two and solving for the imaginary part we come to the conclusion that

$$\kappa_a(\omega) = \frac{\omega}{n(\omega)c}\chi''(\omega), \tag{3.24}$$

and thus

$$\kappa_a(\omega) = \frac{\omega}{n(\omega)c}\mathrm{Im}\int_0^\infty \mathrm{d}t S(t)\exp(i\omega t). \tag{3.25}$$

## 3.3 N-wave mixing experiment

Now that we are familiar with a simple linear absorption experiment and its relation to the linear response function, it is time to extend our theory to involve also the cases of higher order. Firstly we have to realize that the dependence (3.8) of the polarization on the incoming field we postulated is not complete. Let us (for now at least formally) expand the polarization in the orders of the incoming electric field, i.e. we suppose the expansion

$$\vec{P}(\vec{r},t) = \vec{P}^{(1)}(\vec{r},t) + \vec{P}_{NL}(\vec{r},t), \tag{3.26}$$

$$\text{where} \quad \vec{P}_{NL}(\vec{r},t) = \vec{P}^{(2)}(\vec{r},t) + \vec{P}^{(3)}(\vec{r},t) + \ldots,$$

$\vec{P}^{(2)}(\vec{r},t)$ is proportional to $|\vec{E}|^2$, $\vec{P}^{(3)}(\vec{r},t)$ is proportional to $|\vec{E}|^3$ etc. We separated the polarization to linear and non-linear parts. Practically, this means that if we return back to the Maxwell equation (3.7) and invoke the definition (3.11) there will be no zero right-hand side in (3.10) any more. $\vec{P}_{NL}(\vec{r})$ will feature the term that is responsible for the changes of $\vec{E}(\vec{r},t)$. If we assume $\vec{E}(\vec{r},t)$ to be a non-linear signal in a direction of our choice and if we manage to integrate the Maxwell equation with the non-linear term on the right side, we find the desired connection between the detected signal and polarization. Equation we are about to solve has the form

$$\nabla\times\nabla\times\vec{E}(\vec{r},t) + \frac{n^2(\omega)}{c^2}\frac{\partial^2}{\partial t^2}\vec{E}(\vec{r},t) = -\mu_0\frac{\partial^2}{\partial t^2}\vec{P}_{NL}(\vec{r},t). \tag{3.27}$$

Here we made another important assumption, namely we neglected absorption putting absorption coefficient equal to zero, $\kappa_a = 0$, thanks to which $\varepsilon(\vec{k},\omega) = n^2(\omega)$ The whole calculation is going to be much simpler that way without loosing much of its precision. It is common to perform such

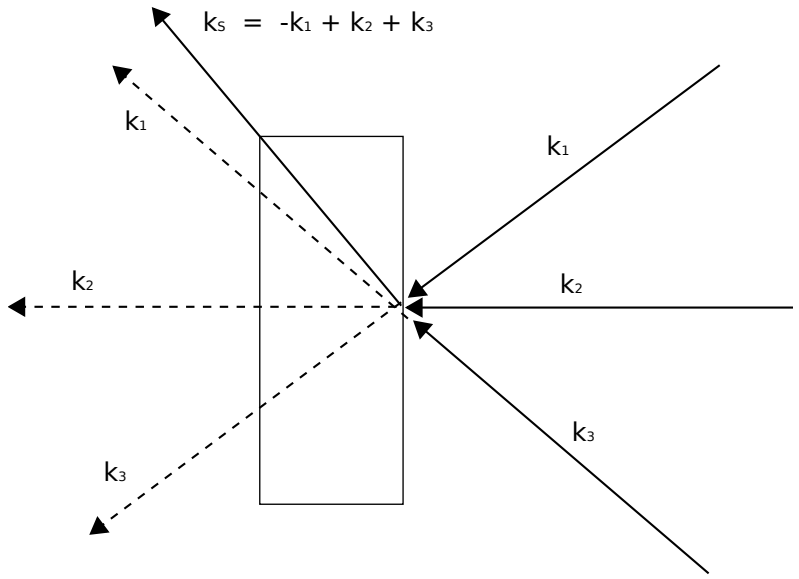


Figure 3.2: 4-wave mixing

experiments under conditions where absorption is kept on minimal possible extent.

Typical experiment where non-linear signal is generated is called *N-wave mixing experiment*. You can see a scheme of this type of experiment on the figure 3.2. By 4-wave mixing we understand three different fields that enter the sample and one non-linear signal leaving the sample in one of the directions given by the directions of the tree incoming pulses. We will represent the electric field corresponding to the incoming modes in the form

$$\vec{E}(\vec{r},t) = \sum_{j=1}^{n-1}[\vec{E}_j(\vec{r},t)\exp(i\vec{k_j}\vec{r} - i\omega_j t) + \vec{E_j}^*(\vec{r},t)\exp(-i\vec{k_j}\vec{r} + i\omega_j t)], \quad (3.28)$$

i.e. in the form of plane waves for all of which we have the same dispersion relation[3]

$$k_j = \frac{\omega_j n_j}{c}. \quad (3.29)$$

Similarly the non-linear polarization could be expanded as follows

$$\vec{P}_{NL}(\vec{r},t) = \sum_{k=2}^{\infty}\sum_{s}\vec{P}_s^{(k)}(t)\exp(i\vec{k}_s\vec{r} - i\omega_s t). \quad (3.30)$$

[3]Again this is only true if $\kappa_a$ is expected to be zero.

[4]Index $k$ indicates the order of polarization and $s$ marks a particular combination of incoming wavevectors and frequencies. It holds

$$\vec{k}_s = \vec{k}_1 \pm \vec{k}_2 \pm \cdots \pm \vec{k}_{n-1} \quad \text{and} \tag{3.31}$$

$$\omega_s = \omega_1 \pm \omega_2 \pm \cdots \pm \omega_{n-1}. \tag{3.32}$$

Let us now restrict our discussion from three to one dimension, we choose a specific direction, let us say along the $z$ axis, and consider a geometry where material occupies a slab of the thickness $l$, $0 < z < l$, $l$ being much larger than the wavelength of radiation beam. This can also be expressed by the condition

$$k_s l \gg 1 \tag{3.33}$$

For maximal simplicity we will not take into account all of the terms of the sum (3.30), but shall focus just on a single Fourier component

$$\vec{P}_{NL}(\vec{r}, t) = \vec{P}_s(t) \exp(ik_s z - i\omega_s t) \tag{3.34}$$

and try to find a solution of the form

$$\vec{E}(\vec{r}, t) = \vec{E}_s(z, t) \exp(ik'_s z - i\omega_s t). \tag{3.35}$$

We further assume that $\vec{P}_s(t)$ is slowly varying in time compared with the optical period

$$\left| \frac{\partial}{\partial t} \vec{P}_s(t) \right| \ll |\omega_s \vec{P}_s(t)|. \tag{3.36}$$

This allows us to rewrite equation (3.27) in this fashion

$$\nabla \times \nabla \times \vec{E}_s(z, t) \exp(ik'_s z) + \frac{n^2(\omega)}{c^2} \vec{E}_s(z, t) \exp(ik'_s z) = -\mu_0 \frac{\partial^2}{\partial t^2} \vec{P}_s(t) \exp(ik_s z), \tag{3.37}$$

where definitions (3.34) and (3.35) were employed, condition (3.36) was respected and all temporal oscillation terms were truncated. The last thing we have to do is to take care of double-rotation term. Recalling the already mentioned property of the field $\nabla \cdot \vec{E}_s(z, t) \exp(ik'_s z) = 0$ we get

$$\nabla \times \nabla \times \vec{E}_s(z, t) \exp(ik'_s z) = -\nabla^2 \vec{E}_s(z, t) \exp(ik'_s z) =$$

[4]Due to the absence of absorption polarization is generated homogeneously throughout the whole sample and thus its magnitude does not change with $\vec{r}$. Only if absorption would be included magnitude would come out to be space dependent.

$$-[\nabla^2\vec{E}(z,t)]\exp(ik'_s z) - 2ik'_s[\nabla\vec{E}_s(z,t)]\exp(ik'_s z) + (k'_s)^2\vec{E}_s(z,t)\exp(ik'_s z).$$

Using the slowly varying amplitude for $\vec{E}_s(z,t)$ we can put $\nabla^2\vec{E}(z,t) \approx 0$ and Maxwell equation will then gain the form

$$ik'_s\frac{\partial\vec{E}_s(z,t)}{\partial z} = -\frac{\omega_s^2}{2c}\vec{P}_s(t)\exp(i\Delta kz) \tag{3.38}$$

with $\Delta k$ denoting the difference between the combination of incoming wavevectors and the wavevector of the generated wave, $\Delta k = k_s - k'_s$. At the beginning of the illuminated sample, at $z = 0$, the intensity of non-linear signal is zero and grows as light moves further and arrives to its peak at the slab interface $z = l$. Therefore, the final intensity of the signal can be obtained by integrating the last equation according to $z$ from 0 to $l$. The result for $\vec{E}_s$ is

$$\vec{E}_s(l,t) = \frac{i}{2n(\omega_s)}\frac{\omega_s}{c}\vec{P}_s(t)\frac{\sin\left(\frac{\Delta kl}{2}\right)}{\left(\frac{\Delta kl}{2}\right)}\exp\left(i\frac{\Delta kl}{2}\right) \tag{3.39}$$

and thus for the intensity we have

$$I_s(l,t) = \frac{cn_s\varepsilon_0}{2}|\vec{E}_s(l,t)|^2 = \frac{\varepsilon_0 c}{8n_s}\omega_s^2 l^2|\vec{P}_s(t)|^2\frac{\sin^2\left(\frac{\Delta kl}{2}\right)}{\left(\frac{\Delta kl}{2}\right)^2}. \tag{3.40}$$

For the limit case when $l \to \infty$ we get

$$I_s(l,t) = \frac{\varepsilon_0 c}{8n_s}\omega_s^2 l^2|\vec{P}_s(t)|^2\delta(\Delta k) \tag{3.41}$$

We have found the answer to the second point of the enumeration on page 38. The only remaining task is to create an efficient microscopic theory for $\vec{P}$. This problem will be dealt with in the section 3.4.

## 3.4 Third order response functions

From this point on we will have to abandon purely macroscopic description and have to use some knowledge of quantum mechanics. Accordingly, density operator has to be presented as a quantum mechanical quantity describing the system. In the following we will not be using the wavefunction $|\psi\rangle$, because it does not posses suitable properties for easy and comfortable mathematical manipulating . Hence we introduce density matrix

$$\hat{\rho} = |\psi\rangle\langle\psi|. \tag{3.42}$$

With the help of $\hat{\rho}$ we are able to define macroscopic polarization as a quantum-mechanical mean value of the polarization operator $\hat{\vec{P}}(\vec{r})$ which is obtained by evaluating the trace of the product of $\hat{\vec{P}}(\vec{r})$ and the density matrix

$$\vec{P}(\vec{r},t) = \mathrm{Tr}\{\hat{\vec{P}}(\vec{r})\hat{\rho}(t)\}, \tag{3.43}$$

where the trace is taken over all possible degrees of freedom that are involved in our description. Polarization operator contains intrinsic information about the treated system and can be expressed in the form of the sum

$$\hat{\vec{P}}(\vec{r}) = \sum_m \hat{\vec{\mathcal{P}}}_m(\vec{r}), \tag{3.44}$$

where $m$ stands for a particular molecule of the sample and by $\hat{\vec{\mathcal{P}}}_m(\vec{r})$ we characterize polarization of this single molecule. This polarization though is given entirely by the transition dipole moment $\hat{\vec{\mu}}_m$ of the molecule[5] $m$ and its position in the coordinate system and thus

$$\hat{\vec{\mathcal{P}}}_m(\vec{r}) = \hat{\vec{\mu}}_m \delta(\vec{r} - \vec{r}_m) \quad \text{with} \quad \hat{\vec{\mu}}_m = \sum_a q_a(\hat{\vec{r}}_a - \vec{R}_m). \tag{3.45}$$

Transition dipole moment operator of a particular molecule $m$ is proportional to the sum over charges $q_a$ of all charged particles multiplied by the operator of their position subtracted by the position of the molecule $m$.

In order to be able to study dynamics of the system we have to specify Hamiltonian which in our case will be comprised of two terms, one that describes the system itself and one that concerns the system-light interaction

$$\hat{H} = \hat{H}_S + \hat{H}_{int}. \tag{3.46}$$

The interaction Hamiltonian is considered to be time dependent. The system part of Hamilton operator however remains stationary. System's dynamics will then be given by equation

$$\frac{\partial}{\partial t}\hat{\rho}(t) = -\frac{i}{\hbar}[(\hat{H}_S + \hat{H}_{int}(t), \hat{\rho}(t)]. \tag{3.47}$$

[5]Since we assume the wavelength of the incoming light to be much larger than the typical size of treated molecules dipole approximation may be applied and our statement holds true. If the wavelength of light and the extend of molecules were of comparable sizes everything would become a little bit more complicated.

While the exact form of $\hat{H}_S$ is not very important at this point, the interaction part has to be determined precisely. Unfortunately, there is no way this Hamiltonian could be derived on concise and elementary basis. We then refer to [11] for sufficiently detailed investigation of this matter. According to [11] we have

$$\hat{H}_S = \hat{H}_{mol} + \hat{V}_{inter} \quad \text{and} \tag{3.48}$$

$$\hat{H}_{int}(t) = -\int \mathrm{d}\vec{r}\hat{\vec{P}}(\vec{r})\vec{E}(\vec{r},t), \tag{3.49}$$

where $\hat{H}_{mol}$ stands for the Hamiltonian of isolated molecules including all of their electronic and nuclear degrees of freedom and $\hat{V}_{inter}$ represents electrostatic interactions between molecules. As you can see we marked polarization with a hat to remind us of the fact that it is the quantum mechanical operator, but left the electric field without this sign. That is because we use so called **semi-classical description of light matter interaction** as many of various spectroscopic techniques are very well and sufficiently described simply by treating electric field as an external parameter, which is purely classical. Though this treatment would not be possible for example for spontaneous emission where non-classical properties of light play an important role, for our purposes this kind of approximation turns up to be fully justified. Therefore $\vec{E}(\vec{r},t)$ is a classical quantity, i.e. the mean value of quantum mechanical field.

Let us now put the definition of polarization operator (3.44) and (3.45) into (3.49) with the result

$$\hat{H}_{int}(t) = -\sum_m \hat{\vec{\mu}}_m \vec{E}(\vec{R}_m,t) \tag{3.50}$$

and if only one single molecule is taken into account

$$\hat{H}_{int}(t) = -\hat{\vec{\mu}}\vec{E}(t) = -\hat{\mu}\vec{n}\vec{E}(t) = -\hat{\mu}E(t), \tag{3.51}$$

where $\vec{n}$ represents a unit vector in the direction of transition dipole moment and scalar $E(t)$ now stand for a projection of the electric field into the direction of the dipole. Thus $\hat{\mu}$ denotes the absolute value of the vector of transition dipole moment.

Before we proceed in our calculations we will implement one further adjustment into our formalism, namely the **superoperator notation**. The implementation of superoperators makes good sense from practical point of view as it makes the theory simpler and briefer. General superoperator $\mathcal{S}$

is a linear operator that acts on a vector space of linear operators. While operators in Hilbert space may be notated in a form of matrices (objects with two indices), superoperators take upon themselves the form of four-dimensional objects with four indices. Nevertheless the linear algebra of superoperators is similar to that of ordinary operators as well as the formal treatment. Most frequently we see superoperators defined as commutators or anti-commutators with the operator they are acting upon. In this fashion we are able to define **Liouville superoperator** (***Liouvillian***) $\mathcal{L}$ as a commutator of Hamiltonian and arbitrary operator $\hat{O}$

$$\mathcal{L}\hat{O} = \frac{1}{\hbar}[\hat{H}, \hat{O}] \tag{3.52}$$

and similarly we define superoperator $\mathcal{V}$ as a commutator of the absolute value of transition dipole operator and arbitrary operator $\hat{O}$

$$\mathcal{V}\hat{O} = \frac{1}{\hbar}[\hat{\mu}, \hat{O}]. \tag{3.53}$$

It is not that easy to show however that for the evolution superoperator $\mathcal{U}(t)$ we have by analogy with the ordinary evolution operator $\hat{U}(t)$

$$\mathcal{U}(t) = \exp(i\mathcal{L}t), \tag{3.54}$$

We refer the reader to [11] where the analysis of this subject can be found. Also without any proof we claim that action of the evolution superoperator is connected with the action of the evolution operator as

$$\mathcal{U}(t)\hat{\rho} = U(t)\hat{\rho}(t)U^{\dagger}(t). \tag{3.55}$$

The equal sign in the last four expressions deserves a little discussion. Since we compare descriptions from two different algebraic spaces we should pay careful attention to its correctness. While superoperators act on Liouville space, operators live in Hilbert space. Although the formal manipulation is very similar and in fact everything we can do in Hilbert space usually holds true in Liouville space as well, there is a peculiarity that is still recommended to have on mind. Both superoperators and operators are ordinarily represented by matrices which means that in one space $\hat{\rho}$ has the form of a vector (Liouville space) and in the other one it bears the form of matrix (Hilbert space). But this formally shows up not to be a problem and the equal sign is indeed fully justified.

So bringing superoperator notation into play equation (3.47) takes the form

$$\frac{\partial}{\partial t}\hat{\rho}(t) = -i\mathcal{L}_S\hat{\rho}(t) - i\mathcal{L}_{int}(t)\hat{\rho}(t) \tag{3.56}$$

and by applying definitions (3.51) and (3.53) we get

$$\frac{\partial}{\partial t}\hat{\rho}(t) = -i\mathcal{L}_S\hat{\rho}(t) + i\mathcal{V}\hat{\rho}(t)E(t), \tag{3.57}$$

which could be transcribed into interaction picture

$$\frac{\partial}{\partial t}\hat{\rho}^{(I)}(t) = i\mathcal{V}^{(I)}(t)\hat{\rho}^{(I)}(t)E(t). \tag{3.58}$$

Here, $\hat{\rho}^{(I)}(t) = \mathcal{U}_S^{\dagger}(t)\hat{\rho}(t)$, where $\mathcal{U}_S(t) = \exp(-i\mathcal{L}_S t)$ is the evolution superoperator with respect to the system and $\mathcal{V}^{(I)}(t) = \mathcal{U}_S^{\dagger}(t)\mathcal{V}\mathcal{U}_S(t)$. This equation can be formally integrated

$$\hat{\rho}^{(I)}(t) = \hat{\rho}^{(I)}(t_0) + i\int_{t_0}^{t} dt'\mathcal{V}^{(I)}(t')\hat{\rho}^{(I)}(t')E(t'), \tag{3.59}$$

while this solution may be inserted into itself which leads us to the form

$$\begin{aligned}\hat{\rho}^{(I)}(t) = \hat{\rho}^{(I)}(t_0) + i\int_{t_0}^{t} dt'\mathcal{V}^{(I)}(t')\hat{\rho}^{(I)}(t_0)E(t') + (i)^2\int_{t_0}^{t} dt'\int_{t_0}^{t'} dt''\mathcal{V}^{(I)}(t')\times \\ \times\mathcal{V}^{(I)}(t'')\hat{\rho}^{(I)}(t_0)E(t')E(t'') + (i)^3\int_{t_0}^{t} dt'\int_{t_0}^{t'} dt''\int_{t_0}^{t''} dt'''\mathcal{V}^{(I)}(t')\times \\ \times\mathcal{V}^{(I)}(t'')\mathcal{V}^{(I)}(t''')\hat{\rho}^{(I)}(t_0)E(t')E(t'')E(t''') + \cdots\end{aligned} \tag{3.60}$$

Now that we found the formal solution for $\hat{\rho}^{(I)}(t)$ it is time to return back from the interaction picture which could be accomplished by applying superoperator $\mathcal{U}_S(t)$ on both sides of the last equation. At the same time we assume that the whole time before we induced the dynamics the system resided in equilibrium state and thus it will make no difference if we send the initial time of the integration $t_0$ to minus infinity, $t_0 \to -\infty$. The result will not change. Then $\hat{\rho}(t_0) = \hat{\rho}^{(I)}(t_0) = \hat{\rho}(-\infty) = \hat{\rho}_{eq}$ will indicate the equilibrium state of the system that remain unchanged under the action of any evolution operator. Under these considerations

$$\hat{\rho}(t) = \hat{\rho}_{eq} + i\int_{-\infty}^{t} dt'\mathcal{U}_S(t)\mathcal{V}^{(I)}(t')E(t')\hat{\rho}_{eq} + (i)^2\int_{-\infty}^{t} dt'\int_{-\infty}^{t'} dt''\mathcal{U}_S(t)\mathcal{V}^{(I)}(t')\times$$

$$\times\mathcal{V}^{(I)}(t'')\hat{\rho}_{eq}E(t')E(t'') + (i)^3\int_{-\infty}^{t}dt'\int_{-\infty}^{t'}dt''\int_{-\infty}^{t''}dt'''\mathcal{U}_S(t)\mathcal{V}^{(I)}(t')\mathcal{V}^{(I)}(t'')\times$$
$$\mathcal{V}^{(I)}(t''')\times\hat{\rho}_{eq}E(t')E(t'')E(t''')+\cdots \tag{3.61}$$

This is very important partial result, because as you see we managed to expand density matrix operator into the orders of incoming electric field, the same thing we did with the macroscopic polarization (see equation (3.26)). In a short time we are going to be able to see the exact microscopic form of both $\vec{P}^{(1)}(\vec{r},t)$ and $\vec{P}^{(3)}(\vec{r},t)$ which are the most relevant orders in the expansion. Consequently, we are going to be able to see the form of $\bar{S}^{(1)}$ and $\bar{S}^{(3)}$. Let us first turn our attention to the first order term, i.e. to the integral

$$\hat{\rho}^{(1)}(t) = i\int_{-\infty}^{t}dt'\mathcal{U}_S(t)\mathcal{U}_S^{\dagger}(t')\mathcal{V}\mathcal{U}_S(t')\hat{\rho}_{eq}E(t'),$$

which could be transferred into the form

$$\hat{\rho}^{(1)}(t) = i\int_{0}^{\infty}\mathrm{d}\tau\mathcal{U}_S(\tau)\mathcal{V}\hat{\rho}_{eq}E(t-\tau),$$

where we employed the substitution $t-t'=\tau$ and used the property of $\hat{\rho}_{eq}$ that it does not evolve in time. Putting this expression into (3.43) and considering only one molecule, i.e. $\hat{\vec{P}}(\vec{r}) = \hat{\vec{\mu}}\delta(\vec{r}-\vec{R})$, we get for first order macroscopic polarization

$$\vec{P}^{(1)}(\vec{r},t) = i\int_{0}^{\infty}\mathrm{d}\tau\mathrm{Tr}\left\{\hat{\vec{\mu}}\mathcal{U}_S(\tau)\mathcal{V}\hat{\rho}_{eq}\right\}E(t-\tau). \tag{3.62}$$

If we now compare this equation with (3.8), the definition of linear polarization through first order response function, we find out that

$$\bar{S}^{(1)}(t) = \frac{i}{\hbar}\mathrm{Tr}\left\{\hat{\vec{\mu}}\mathcal{U}_S(t)[\hat{\mu},\hat{\rho}_{eq}]\right\} \tag{3.63}$$

Since the response for negative times does not have any physical interpretation we will make a correction. We use the Heaviside step function $\Theta(t)=1$ for $t>0$ and $\Theta(t)=0$ for $t<0$ and the final form would then be

$$\bar{S}^{(1)}(t) = \Theta(t)\frac{i}{\hbar}\mathrm{Tr}\left\{\hat{\vec{\mu}}\mathcal{U}_S(t)[\hat{\mu},\hat{\rho}_{eq}]\right\}. \tag{3.64}$$

The manipulation with third order term is a little more complex. This time we have a triple integral to rearrange

$$\hat{\rho}^{(3)}(t) = (i)^3 \int_{-\infty}^{t} \mathrm{d}t' \int_{-\infty}^{t'} \mathrm{d}t'' \int_{-\infty}^{t''} \mathrm{d}t''' \mathcal{U}_S(t-t')\mathcal{V}\mathcal{U}_S(t'-t'')\times$$
$$\times \mathcal{V}\mathcal{U}_S(t''-t''')\mathcal{V}\mathcal{U}_S(t''')\hat{\rho}_{eq}E(t')E(t'')E(t'''), \tag{3.65}$$

where again we change some variables and use the stationary property of the equilibrium density matrix. Let us put $t_3 = t - t'$, $t_2 = t' - t'' = t - t_3 - t''$ and $t_1 = t'' - t''' = t - t_3 - t_2 - t'''$ which leads us to

$$\hat{\rho}^{(3)}(t) = (i)^3 \int_0^{\infty} \mathrm{d}t_3 \int_0^{\infty} \mathrm{d}t_2 \int_0^{\infty} \mathrm{d}t_1 \mathcal{U}_S(t_3)\mathcal{V}\mathcal{U}_S(t_2)\mathcal{V}\mathcal{U}_S(t_1)\mathcal{V}\times$$
$$\times \hat{\rho}_{eq}E(t-t_3)E(t-t_2-t_3)E(t-t_1-t_2-t_3). \tag{3.66}$$

We have not strictly defined third order polarization yet. From the analogy with the first order term we can define

$$\vec{P}^{(3)}(\vec{r},t) = \int_0^{\infty} \mathrm{d}t_3 \int_0^{\infty} \mathrm{d}t_2 \int_0^{\infty} \mathrm{d}t_1 \bar{S}^{(3)}(t_3,t_2,t_1)\times$$
$$\times E(t-t_3)E(t-t_2-t_3)E(t-t_1-t_2-t_3) \tag{3.67}$$

thus finally arriving to the expression in the form

$$\bar{S}^{(3)}(t_3,t_2,t_1) = (i)^3 \mathrm{Tr}\left\{\hat{\vec{\mu}}\mathcal{U}_S(t_3)\mathcal{V}\mathcal{U}_S(t_2)\mathcal{V}\mathcal{U}_S(t_1)\mathcal{V}\hat{\rho}_{eq}\right\}. \tag{3.68}$$

Again we do a correction and exclude all negative times to obtain

$$\bar{S}^{(3)}(t_3,t_2,t_1) = (i)^3\Theta(t_3)\Theta(t_2)\Theta(t_1)\mathrm{Tr}\left\{\hat{\vec{\mu}}\mathcal{U}_S(t_3)\mathcal{V}\mathcal{U}_S(t_2)\mathcal{V}\mathcal{U}_S(t_1)\mathcal{V}\hat{\rho}_{eq}\right\}. \tag{3.69}$$

Apparently, as simple as this expression may seem it in fact comprises of 8 different terms since the $\mathcal{V}$ superoperator is defined as a commutator and it acts on everything that stands on the right from it. One commutator would give two terms, which means that in general $n$ superoperators in the expression would lead to the sum of $2^n$ addends. It could be demonstrated though that each term has its complex conjugated partner and thus equation (3.68) could be written as a sum of four functions plus their complex conjugates

$$\bar{S}^{(3)}(t_3,t_2,t_1) = \left(\frac{i}{\hbar}\right)^3 \sum_{k=1}^{4} \left[R_k(t_3,t_2,t_1) - R_k^*(t_3,t_2,t_1)\right]. \tag{3.70}$$

where $R_1(t_3,t_2,t_1),\ldots,R_4(t_3,t_2,t_1)$ are defined as

$$R_1(t_3,t_2,t_1) = \mathrm{Tr}\left\{\hat{\mu}(t_1)\hat{\mu}(t_1+t_2)\hat{\mu}(t_1+t_2+t_3)\hat{\mu}(0)\hat{\rho}_{eq}\right\}, \tag{3.71}$$

$$R_2(t_3,t_2,t_1) = \mathrm{Tr}\left\{\hat{\mu}(0)\hat{\mu}(t_1+t_2)\hat{\mu}(t_1+t_2+t_3)\hat{\mu}(t_1)\hat{\rho}_{eq}\right\}, \tag{3.72}$$

$$R_3(t_3,t_2,t_1) = \mathrm{Tr}\left\{\hat{\mu}(0)\hat{\mu}(t_1)\hat{\mu}(t_1+t_2+t_3)\hat{\mu}(t_1+t_2)\hat{\rho}_{eq}\right\}, \tag{3.73}$$

$$R_4(t_3,t_2,t_1) = \mathrm{Tr}\left\{\hat{\mu}(t_1+t_2+t_3)\hat{\mu}(t_1+t_2)\hat{\mu}(t_1)\hat{\mu}(0)\hat{\rho}_{eq}\right\}. \tag{3.74}$$

where we introduced time dependent dipole moment operator that is defined as

$$\hat{\mu}(t) = \mathcal{U}_S^{\dagger}(t)\hat{\mu} = U_S^{\dagger}(t)\hat{\mu}U_S(t), \tag{3.75}$$

which is also a definition of the interaction picture of the operator $\hat{\mu}$. The equations (3.71)-(3.74) are so called Liouville pathways and they fully define the third order response function. The higher orders would be calculated exactly in the same fashion with the only change in the number of the $\mathcal{V}$ superoperators acting on the equilibrium density matrix operator $\hat{\rho}_{eq}$ and consequently the number of final Liouville pathways (16 for 4th order, 32 for the 5th order etc.). These higher orders are used rather exceptionally. The next section will be dedicated to a brief description of how we got from (3.68) to (3.70) and the common notation and depiction of the $R$ functions.

## 3.5 Liouville pathways

Let us get back to the equation (3.68) for the third order response function for a while. We know already that it comprises 8 different terms, because the $\mathcal{V}$ superoperator has the form of commutator. Each commutator contains two terms, one where the operator acts from the left and one where it acts from the right. This means that the 8 functions we are interested in are merely the combinations of several possibilities where operators act from left or right in different fashion. In order to be more specific about this we rewrite (3.68) in the language of commutators.

$$\bar{S}^{(3)}(t_3,t_2,t_1) = (i)^3\mathrm{Tr}\left\{\hat{\tilde{\mu}}\mathcal{U}_S(t_3)\Big[\hat{\mu},\mathcal{U}_S(t_2)\big[\hat{\mu},\mathcal{U}_S(t_1)[\hat{\mu},\hat{\rho}_{eq}]\big]\Big]\right\} \tag{3.76}$$

Even more precisely we should transfer the evolution superoperator to the operator representation too. That would lead to

$$\bar{S}^{(3)}(t_3,t_2,t_1) =$$

$$= (\frac{i}{\hbar})^3 \mathrm{Tr}\left\{\hat{\vec{\mu}} U_S(t_3)\Big[\hat{\mu}, U_S^\dagger(t_2)\big[\hat{\mu}, U_S(t_1)[\hat{\mu}, \hat{\rho}_{eq}]U_S^\dagger(t_1)\big]U_S^\dagger(t_2)\Big]U_S^\dagger(t_3)\right\}. \tag{3.77}$$

Here we choose one particular function, let us say $R_1$ and provide a deeper analysis. The treatment of the remaining functions would be a pure analogy of what we show now. It comes from a convention that the $R_1$ functions corresponds to the case where transition dipole moment operator $\hat{\mu}$ acts first from the left, then twice from the right and finally from the left again (this last action is the same for all functions and reflects the definition). Hence we have

$$R_1^{(3)}(t_3, t_2, t_1) = \mathrm{Tr}\left\{\hat{\vec{\mu}} U_S(t_3)U_S(t_2)U_S(t_1)\hat{\mu}\hat{\rho}_{eq}U_S^\dagger(t_1)\hat{\mu}U_S^\dagger(t_2)\hat{\mu}U_S^\dagger(t_3)\right\} \tag{3.78}$$

and using the cycling invariance of the trace operator we can rearrange everything so that the $\hat{\rho}_{eq}$ goes to the very right position of the trace. After doing that we expand the expression by insertion the unit operator in the appropriate form, which would be here $1 = U(t)U^\dagger(t)$. This way we get to the conclusion

$$R_1^{(3)}(t_3, t_2, t_1) = \mathrm{Tr}\Big\{U_S^\dagger(t_1)\hat{\mu}U_S(t_1)U_S^\dagger(t_1 + t_2)\times$$

$$\times\hat{\mu}U_S(t_1 + t_2)U_S^\dagger(t_1 + t_2 + t_3)\hat{\vec{\mu}}U_S(t_1 + t_2 + t_3)\hat{\mu}\hat{\rho}_{eq}\Big\} \tag{3.79}$$

which is exactly Eq. (3.71).

Schematically we can represent the $R_1$ pathway using a Feynman diagram (see Fig. 3.3 – on the left) that transparently shows its whole structure. It looks a bit like a ladder at the bottom of which we can imagine the beginning of the time axis and at the top its end. We may further consider each rung a moment where $\hat{\mu}$ acts on $\hat{\rho}_{eq}$ and induces a certain dynamics by changing the current state of density matrix. We also notice that each action of $\hat{\mu}$ is followed by the system's time evolution given by the operator $\mathcal{U}_S(t)$ and of course the arrows indicate the side from which dipole moment operator comes into action. Another representation of Liouville pathways is depicted on the left side of the Fig. 3.3. The meaning of this scheme is that if $\hat{\mu}$ acts from the left we move vertically and if $\hat{\mu}$ acts from the right we move horizontally. Feynman diagrams and the corresponding schemes of the remaining pathways are shown in figures 3.4,3.5 and 3.6. Using this symbolic notation is very comfortable and in case we would need it is always possible to reconstruct the original formal mathematical objects.

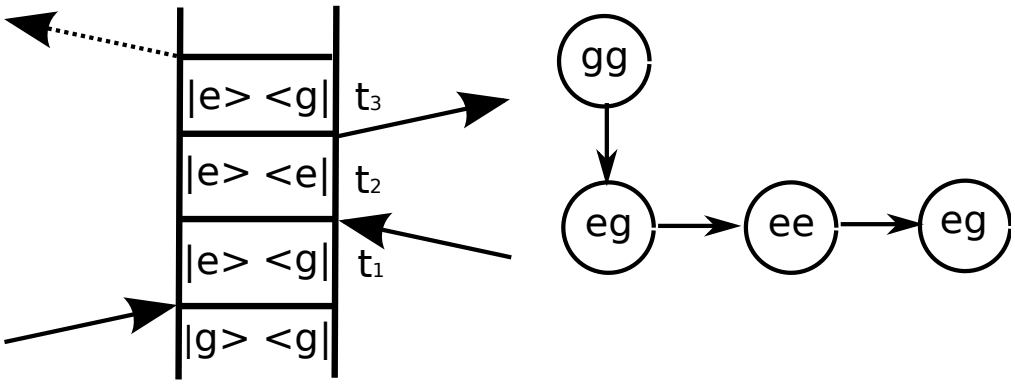


Figure 3.3: Feynman diagram and a schematic depiction of the Liouville pathway $R_1$ for a two-level system. This pathway goes through the system's **excited** state.

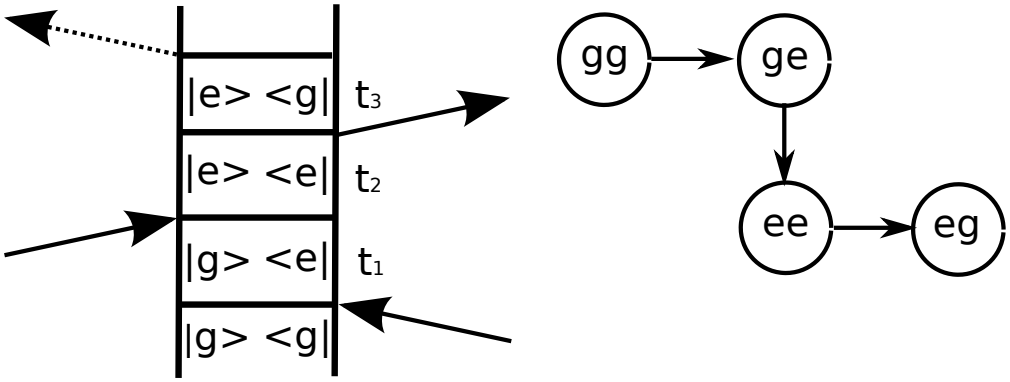


Figure 3.4: Feynman diagram and a schematic depiction of the Liouville pathway $R_2$ for a two-level system. This pathway goes through the system's **excited** state.

One other thing we have to mention here is that all the four diagrams and schemes in the above mentioned pictures are shown for a two-level system with only one excited state. The other diagrams for a multilevel systems could be derived as well, but it would be a subject for another chapter which unfortunately lays beyond intentions of this short introduction. But we still owe an explanation on the account of the factual evolution of the two-level system according the particular Liouville pathways and that is what we would like to dedicate the following paragraph to.

Hamiltonian of the two-level system may be expressed in a diagonal form

$$\hat{H}_S = \hat{H}_g \left|g\right\rangle \left\langle g\right| + \hat{H}_e \left|e\right\rangle \left\langle e\right| . \tag{3.80}$$

Therefore the evolution operator of the system also takes upon itself the diagonal form

$$\hat{U}_S(t) = U_g \left|g\right\rangle \left\langle g\right| + U_e \left|e\right\rangle \left\langle e\right| . \tag{3.81}$$

Transition dipole operator on the other hand is anti-diagonal and reads

$$\hat{\mu} = d_{ge} \left|g\right\rangle \left\langle e\right| + d_{eg} \left|e\right\rangle \left\langle g\right| . \tag{3.82}$$

where $d_{ge}$ and $d_{eg}$ are complex numbers which satisfy relation $d^*_{ge} = d_{eg}$, i.e. are mutually complex conjugated. Finally we have to express density matrix and we assume that in the initial phase it consists of a single non-zero term that refer to the ground state

$$\hat{\rho}_{eq} = \rho_{gg} \left|g\right\rangle \left\langle g\right| . \tag{3.83}$$

Let us now follow step by step the pathway $R_1$ (Fig. 3.3) and imagine what happens when transition dipole moment operator acts from the left on the equilibrium density matrix. In the matrix notation we have

$$\hat{\mu}\hat{\rho}_{eq} = \begin{pmatrix} 0 & d_{ge} \\ d_{eg} & 0 \end{pmatrix} \begin{pmatrix} \rho_{gg} & 0 \\ 0 & 0 \end{pmatrix} = \begin{pmatrix} 0 & 0 \\ d_{eg}\rho_{gg} & 0 \end{pmatrix} = d_{eg}\rho_{gg} \left|e\right\rangle \left\langle g\right| ,$$

and as we see density matrix has been brought from the ground state to one of the coherence states which indeed agrees with the state that occupies the first rung of the $R_1$-Feynman diagram. After this there comes an evolution in time, more precisely the evolution from some initial time $t_0$ to time $t_1$. But since the evolution operator bears a diagonal form the will be no changes as far as the state of density matrix is concerned.

$$U_S(t_1)\hat{\mu}\hat{\rho}_{eq}U_S^{\dagger}(t_1) = \begin{pmatrix} e^{-\frac{i}{\hbar}\hat{H}_g t} & 0 \\ 0 & e^{-\frac{i}{\hbar}\hat{H}_e t} \end{pmatrix} \begin{pmatrix} 0 & 0 \\ d_{eg}\rho_{gg} & 0 \end{pmatrix} \begin{pmatrix} e^{+\frac{i}{\hbar}\hat{H}_g t} & 0 \\ 0 & e^{+\frac{i}{\hbar}\hat{H}_e t} \end{pmatrix}$$

$$= \begin{pmatrix} 0 & 0 \\ e^{-\frac{i}{\hbar}\hat{H}_e t} d_{eg} \rho_{gg} e^{+\frac{i}{\hbar}\hat{H}_g t} & 0 \end{pmatrix} = e^{-\frac{i}{\hbar}\hat{H}_e t} d_{eg} \rho_{gg} e^{+\frac{i}{\hbar}\hat{H}_g t} |e\rangle \langle g|$$

The next action of $\hat{\mu}$ comes from the right and it should bring the density matrix into the excited state. This is really true as we know that

$$U_S(t_1)\hat{\mu}\hat{\rho}_{eq}U_S^\dagger(t_1)\hat{\mu} = \begin{pmatrix} 0 & 0 \\ e^{-\frac{i}{\hbar}\hat{H}_e t} d_{eg} \rho_{gg} e^{+\frac{i}{\hbar}\hat{H}_g t} & 0 \end{pmatrix} \begin{pmatrix} 0 & d_{ge} \\ d_{eg} & 0 \end{pmatrix} =$$

$$= |d|^2 \begin{pmatrix} 0 & 0 \\ 0 & e^{-\frac{i}{\hbar}\hat{H}_e t} \rho_{gg} e^{+\frac{i}{\hbar}\hat{H}_g t} \end{pmatrix} \rho_{gg} |e\rangle \langle e| .$$

Hopefully this puts some more light into the presented form of Feynman diagrams. From now on as the expression in the matrices get more and more complicated we afford to simplify the notation and for every non-zero term just use the symbol $\bullet$. It is not hard to see that

$$U_S(t_2)U_S(t_1)\hat{\mu}\hat{\rho}_{eq}U_S^\dagger(t_1)\hat{\mu}U_S(t_2) = \begin{pmatrix} \bullet & 0 \\ 0 & \bullet \end{pmatrix} \begin{pmatrix} 0 & 0 \\ 0 & \bullet \end{pmatrix} \begin{pmatrix} \bullet & 0 \\ 0 & \bullet \end{pmatrix} = \begin{pmatrix} 0 & 0 \\ 0 & \bullet \end{pmatrix}$$

and

$$U_S(t_2)U_S(t_1)\hat{\mu}\hat{\rho}_{eq}U_S^\dagger(t_1)\hat{\mu}U_S(t_2)\hat{\mu} = \begin{pmatrix} 0 & 0 \\ 0 & \bullet \end{pmatrix} \begin{pmatrix} 0 & \bullet \\ \bullet & 0 \end{pmatrix} = \begin{pmatrix} 0 & 0 \\ \bullet & 0 \end{pmatrix}$$

After this there again follows one more time evolution and that is where the Liouville pathway comes to an end.

## 3.6 Pulsed experiments

Now that we learned about Liouville pathways, we are able to derive even more complete form of the third order polarization. In order to do that we refer to the 4-wave mixing experiment showed in the Fig. 3.2. Let us look at it in a slightly different perspective. The three incoming pulses do not enter the sample simultaneously, but there are defined time delays between them. This fact is demonstrated in the Fig. 3.7 where the pulses are numbered with respect to the order in which they get to the sample. They might be described as plain waves allowing us to write the total incoming field in the form

$$E(\vec{r},t) = A_1(t+T+\tau)e^{-i\omega_1(t+T+\tau)+i\vec{k}_1\vec{r}} + A_2(t+T)e^{-i\omega_2(t+T)+i\vec{k}_2\vec{r}} +$$

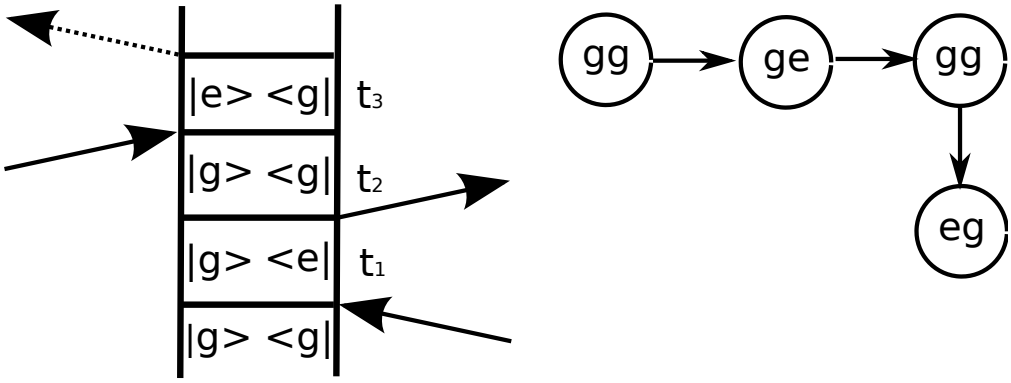


Figure 3.5: Feynman diagram and a schematic depiction of the Liouville pathway $R_3$ for a two-level system. This pathway goes through the system's **ground** state.

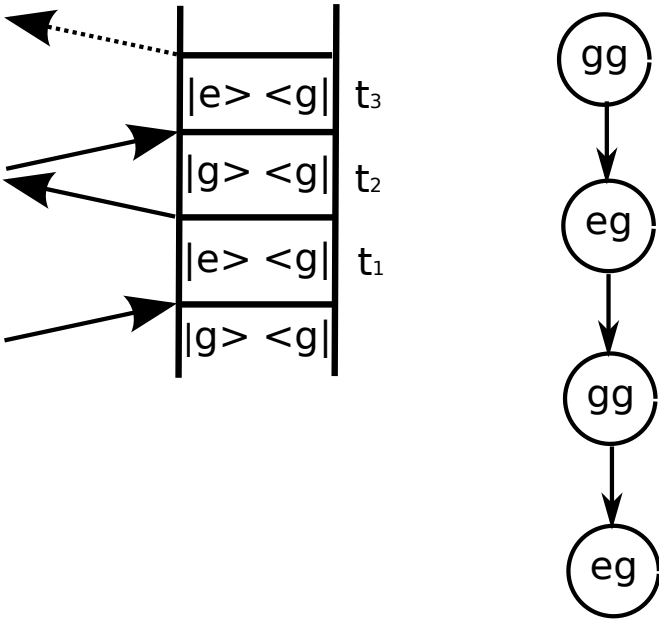


Figure 3.6: Feynman diagram and a schematic depiction of the Liouville pathway $R_4$ for a two-level system. This pathway goes through the system's **ground** state.

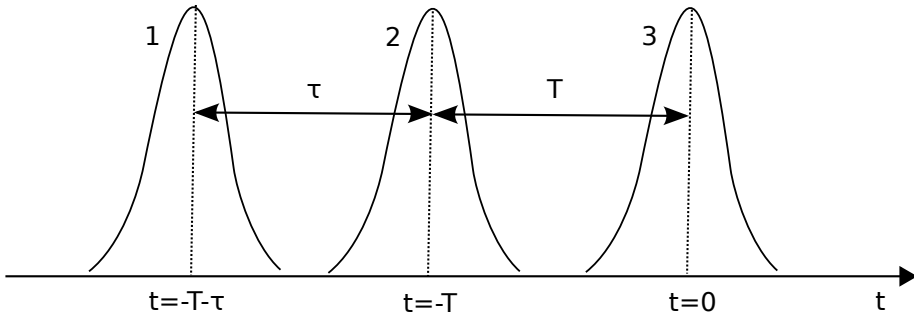


Figure 3.7: Depiction of three pulses entering the 4-wave mixing experiment along with the delay times between them.

| | $E(t-t_3)$ | $E(t-t_2-t_3)$ | $E(t-t_1-t_2-t_3)$ |
|---|---|---|---|
| I | $1^*$ | 2 | 3 |
| II | $1^*$ | 3 | 2 |
| III | 2 | $1^*$ | 3 |
| IV | 3 | $1^*$ | 2 |
| V | 2 | 3 | $1^*$ |
| VI | 3 | 2 | $1^*$ |

Table 3.1: Six possible contributions to non-linear signal in the direction $-\vec{k}_1+\vec{k}_2+\vec{k}_3$. Numbers 1,2 and 3 denote the corresponding plain wave from Eq. (3.84), stars in the upper index indicate that the complex conjugate term of the wave is used.

$$+A_3(t)e^{-i\omega_3 t+i\vec{k}_3\vec{r}}+c.c. \tag{3.84}$$

At this point we make use of the Eq. (3.67) for the third order polarization and see what happens if this form of total field is applied to it. Since the electric field appears three times in the definition of third order polarization and the expression for the total field consists of six terms, we would have to deal with $6\times 6\times 6$ terms. But this number could be considerably reduced by looking only at the signal in one particular direction. Let this direction be $-k_1+k_2+k_3$ which is a prominent direction used in many applications. By doing that there remain 6 terms, which we schematically arranged in the table 3.1 and assigned to roman numerals I-VI. To avoid any misunderstandings we write the term VI explicitly, it reads

$$A_1^*(t+T+\tau-t_3-t_2-t_1)e^{i\omega(t+T+\tau-t_3-t_2-t_1)}A_2(t+T-t_2-t_3)e^{-i\omega(t+T-t_2-t_3)}\times$$

| | | |
|---|---|---|
| I | $-i\omega(t-\tau)+i\omega(t_1+2t_2+t_3)$ | DC |
| II | $-i\omega(t-\tau)+i\omega(t_1+2t_2+t_3)$ | DC |
| III | $-i\omega(t-\tau)+i\omega(t_1+t_3)$ | NR |
| IV | $-i\omega(t-\tau)+i\omega(t_1+t_3)$ | NR |
| V | $-i\omega(t-\tau)+i\omega(t_3-t_1)$ | R |
| VI | $-i\omega(t-\tau)+i\omega(t_3-t_1)$ | R |

Table 3.2: Phases of six possible contributions to non-linear signal.

$$\times A_3(t-t_3)e^{-i\omega(t-t_3)} =$$
$$= A_1^*(t+T+\tau-t_3-t_2-t_1)A_2(t+T-t_2-t_3)A_3(t-t_3)e^{-i\omega(t-\tau)+i\omega(t_3-t_1)}. \quad (3.85)$$

As you can see the term is characterized by its phase factor $e^{i\phi}$, $\phi$ being the phase, in this case it is the factor $e^{-i\omega(t-\tau)+i\omega(t_3-t_1)}$, which is termed **Rephasing** (R). The other factors are known as **Non-Rephasing** (NR) and **Double Coherence** (DC). The amplitudes are not so important for us at this stage. The corresponding phase factors of the rest of the terms are included in the table 3.2.

Our next step would be to closer investigate the four Liouville pathways. We shall use the first pathway $R_1$ as an example for which in the previous section we derived the form

$$R_1^{(3)}(t_3,t_2,t_1) = \mathrm{Tr}\left\{\hat{\tilde{\mu}}U_S(t_3)U_S(t_2)U_S(t_1)\hat{\mu}\hat{\rho}_{eq}U_S^\dagger(t_1)\hat{\mu}U_S^\dagger(t_2)\hat{\mu}U_S^\dagger(t_3)\right\},$$

(see Eq. (3.78)). The evolution operator in this equation may be expressed according to Eq. (3.81) and dipole operator has been defined by Eq. (3.82), which allows us to perform the trace operation over electronic degrees of freedom. This operation leads to

$$R_1^{(3)}(t_3,t_2,t_1) = |d|^4\mathrm{Tr}_{\mathrm{Bath}}\left\{U_e(t_3)U_e(t_2)U_e(t_1)\hat{\rho}_{eq}U_g^\dagger(t_1)U_e^\dagger(t_2)U_g^\dagger(t_3)\right\}. \quad (3.86)$$

The operators $U_g$, $U_e$ may be divided into two parts describing system and bath separately, i.e.

$$U_g(t) = e^{-\frac{i}{\hbar}\varepsilon_g t}\tilde{U}_g(t), \quad (3.87)$$

where $\varepsilon_g$ stands for the energy of the ground state and $\tilde{U}_g(t)$ is the evolution operator with respect to the bath degrees of freedom. Similarly

$$U_e(t) = e^{-\frac{i}{\hbar}\varepsilon_e t}\tilde{U}_e(t), \quad (3.88)$$

| L. pathway | phase $\phi$ | |
|---|---|---|
| $R_1$ | $-i\omega_{eg}(t_1+t_3)$ | NR |
| $R_2$ | $-i\omega_{eg}(t_3-t_1)$ | R |
| $R_3$ | $-i\omega_{eg}(t_3-t_1)$ | R |
| $R_4$ | $-i\omega_{eg}(t_1+t_3)$ | NR |

Table 3.3: Phase factors $e^{i\phi}$of the four Liouville pathways.

$\varepsilon_e$ denoting the energy of excited state. Now by taking the last three expressions together we are able to determine the phase factor of $R_1$. After making all the necessary rearrangements we get

$$R_1^{(3)}(t_3,t_2,t_1) =$$

$$= |d|^4 e^{-i\omega_{eg}(t_1+t_3)} \mathrm{Tr}_{\mathrm{Bath}} \left\{ \tilde{U}_e(t_3)\tilde{U}_e(t_2)\tilde{U}_e(t_1)\hat{\rho}_{eq}\tilde{U}_g^\dagger(t_1)\tilde{U}_e^\dagger(t_2)\tilde{U}_g^\dagger(t_3) \right\} =$$

$$= |d|^4 e^{-i\omega_{eg}(t_1+t_3)} \tilde{R}_1(t_3,t_2,t_1) \tag{3.89}$$

with $\omega_{eg} = \frac{1}{\hbar}(\varepsilon_e - \varepsilon_g)$. It will surely not be surprising that the phase factor we obtained is very similar to some of those in the table 3.2. In fact, they are the same, but the sign is different. The phase factors for all four Liouville pathways are listed in the table.

Now, we can say that the third order polarization on one hand contains terms that does not change much in time, or change relatively slowly (amplitudes of the fields, $\tilde{R}$) and on the other hand includes phase factors that change relatively rapidly (with optical frequencies). If the frequencies $\omega$ and $\omega_{eg}$ were the same or at least very near to each other (we could also say that the frequency of the incoming laser pulses are in resonance with the optical transition), the phase factors with opposite signs would cancel and the integrand in (3.67) would not oscillate in the process of integration. It would thus give a non-zero contribution. On the contrary if the phase factors would take part in the integration, the oscillations would be simply too fast and the result would be nearly zero. The condition $\omega \approx \omega_{eg}$ allows us to neglect all the fast oscillating terms, which is called **Rotating Wave Approximation** (RWA). If we apply this approximation we find out that the only non-zero contributions to the integral (3.67) are those where the terms V or VI meet with $R_2$ or $R_3$ and those where terms III or IV meet

with $R_1$ or $R_4$. Therefore, we have

$$\vec{P}(\vec{r},t) = \left(\frac{i}{\hbar}\right)^3 \int_0^\infty \mathrm{d}t_3 \int_0^\infty \mathrm{d}t_2 \int_0^\infty \mathrm{d}t_3 \Big\{ \left[\tilde{R}_2(t_3,t_2,t_1) + \tilde{R}_3(t_3,t_2,t_1)\right] \times$$
$$\times \left[\mathrm{V} + \mathrm{VI}\right] e^{i(\omega-\omega_{eg})(t_3-t_1)} + \left[\tilde{R}_1(t_3,t_2,t_1) + \tilde{R}_4(t_3,t_2,t_1)\right] \times$$
$$\times \left[\mathrm{III} + \mathrm{IV}\right] e^{i(\omega-\omega_{eg})(t_3+t_1)} \Big\} e^{-i\omega(t-\tau)}. \tag{3.90}$$

Finally, let us return for a moment to Eq. (3.85) that describes the form of VI from the last equation and let us assume that the incoming laser pulses are infinitely short, so that we can write $A(t) = \delta(t)$. This presumption implies $t_3 = t$, $t_2 = T$ and $t_1 = \tau$. Obviously, all three times are positive. But when do same thing with the terms III, IV and V we get negative values for time $t_1$ or $t_2$ which is course in conflict with the limits of the integration. For this reason, not even these terms contribute to the polarization and we may conclude that

$$\vec{P}(\vec{r},t) = \left(\frac{i}{\hbar}\right)^3 e^{-i\omega_{eg}(t-\tau)} \left[\tilde{R}_2(t,T,\tau) + \tilde{R}_3(t,T,\tau)\right]. \tag{3.91}$$

This means that only rephasing Liouville pathways give non-zero signal. But there is a way to get signal from non-rephasing parts as well. Let us suppose we change the sing of the delay time $\tau$ which would effectively lead to reversing the order of first and second pulses, i.e. the second pulse would strike in the system before the first pulse. Surely, this is something we can do without loosing physical meaning of our calculations. But suddenly the time $t_1$ in our example would become negative. It could be shown that in this case only non-rephasing pathways would create the signal which could be expressed by following equation

$$\vec{P}(\vec{r},t) = \left(\frac{i}{\hbar}\right)^3 e^{-i\omega_{eg}(t+\tau)} \left[\tilde{R}_1(t,T,-\tau) + \tilde{R}_4(t,T,-\tau)\right]. \tag{3.92}$$

## 3.7 Heterodyne detection

The generation of non-linear signal through wave mixing has one great advantage and that is the possibility of sending the outgoing signal into the new direction, different from that of incoming waves. Thanks to this fact

there are no background effects in the detection of such a signal. Despite this advantage the non-linear signal is still very weak to detect, mostly because of the quadratic dependence of measured intensity on polarization, equation (3.40). Nevertheless, this little drawback could be easily obviated if we turn to so called *heterodyne detection*. This means that we use another field with the wavevector aiming in the same direction as the detected signal, which we usually denote $E_{LO}$ – the **local oscillator** field. It holds that this additional field is much stronger than the weak non-linear signal, i.e. $E_{LO} \gg E_S$. After the signal passes through the sample we now observe the superposition of the local oscillator field and the signal field resulting in the total detected intensity

$$I_T = \varepsilon_0 n(\omega) c |E_{LO}(t) + E_s(t)|^2 = I_{LO}(t) + I_s(t) + 2I_{HET}(t). \tag{3.93}$$

$I_{LO}$ represents the intensity of the local oscillator field alone and $I_{HET}$ stands for the mixed, heterodyne signal for which we have

$$I_{HET}(t) = \varepsilon_0 n(\omega) c \mathrm{Re}[E^*_{LO}(t) E_s(t)]. \tag{3.94}$$

From the requirement on local oscillator field being much stronger than detected signal, the second term in the last equation becomes negligible in comparison with the remaining two. Then the first term is known and could be subtracted and thus all important information is included in the third term. The main advantage is evident from the first sight, we managed to reduce the quadratic dependence of signal on polarization to plain linear. This ensures much easier detection of weak non-linear signal. Besides, by controlling the relative phase of $E_{LO}$ and $P_s$ it becomes possible to probe separately the real and imaginary parts of polarization, resulting in a phase sensitive detection. If we use a simplified version of equation (3.39) it will turn out that the intensity is given by

$$I(t) = \varepsilon_0 n(\omega) c \mathrm{Re}[E^*_{LO}(t) E_s(t)] = ... - \omega l \mathrm{Im}[E^*_{LO}(t) P_s(t)]. \tag{3.95}$$

On the top of all if the signal is generated along the direction of one of the incoming beams the heterodyne detection occurs intrinsically. This is domain of such methods as stimulated Raman or photon echo, and of course pump-probe. In case of the latter one we prove our statement in the next section.

## 3.8 Detection of pump-probe signal

Let us start our thinking about pump probe experiment by trying to find what energy gets absorbed in the process of probing. In other words we want to find the amount of energy added to the matter (or lost by the field). Energy absorbed at a time $t$ after the incidence of the light beam may be defined as a trace over Hamiltonian operator acting on density matrix

$$< W(t) >= \mathrm{Tr}\left\{\hat{H}(t)\hat{\rho}(t)\right\}, \tag{3.96}$$

which could be formally differentiated according to $t$

$$\frac{\mathrm{d}}{\mathrm{d}t} < W(t) >= \mathrm{Tr}\left\{\left(\frac{\mathrm{d}}{\mathrm{d}t}\hat{H}_{int}(t)\right)\hat{\rho}\right\} + \mathrm{Tr}\left\{\hat{H}(t)\left(\frac{\mathrm{d}}{\mathrm{d}t}\hat{\rho}(t)\right)\right\}. \tag{3.97}$$

Since our Hamiltonian is by the definition (3.46) divided into the stationary system part $\hat{H}_S$ and the time dependent interaction part $\hat{H}_{int}(t)$ the time derivative of the system part gives zero and remains only the second term. As a next step we employ Heisenberg equation (3.47) which implies the second trace in the last equation to be zero, $-\frac{i}{\hbar}\mathrm{Tr}\left\{\hat{H}(t)\hat{H}(t)\hat{\rho}(t) - \hat{H}(t)\hat{\rho}(t)\hat{H}(t)\right\} = -\frac{i}{\hbar}\mathrm{Tr}\left\{\hat{H}(t)\hat{H}(t)\hat{\rho}(t) - \hat{H}(t)\hat{H}(t)\hat{\rho}(t)\right\} = 0$[6]. Now we include interaction Hamiltonian (3.49), it yields

$$\frac{\mathrm{d}}{\mathrm{d}t} < W(t) >= -\int_{-\infty}^{+\infty} \mathrm{d}\vec{r}\left[\frac{\partial}{\partial t}\vec{E}(\vec{r},t)\right]\vec{P}(\vec{r},t). \tag{3.98}$$

Lastly we have to express electric field and polarization in some way. As we did in the section about N-wave mixing we write both fields in the form of a plain wave.

$$\vec{E}(\vec{r},t) = \vec{E}(t)\exp(i\vec{k}\vec{r} - i\omega t) + \vec{E}^*(t)\exp(-i\vec{k}\vec{r} + i\omega t), \tag{3.99}$$

$$\vec{P}(\vec{r},t) = \vec{P}_s(t)\exp(i\vec{k}_s\vec{r} - i\omega t) + \vec{P}_s^*(t)\exp(-i\vec{k}_s\vec{r} + i\omega t). \tag{3.100}$$

[6] We made use of the property of trace called *cyclic invariance* stating that for any two arbitrary operators $\hat{O}$, $\hat{P}$ we have $\mathrm{Tr}\left\{\hat{O}\hat{P}\right\} = \sum_a \langle a|\hat{O}\hat{P}|a\rangle = \sum_{a,b}\langle a|\hat{O}|b\rangle\langle b|\hat{P}|a\rangle = \sum_{a,b}\langle b|\hat{P}|a\rangle\langle a|\hat{O}|b\rangle = \mathrm{Tr}\left\{\hat{P}\hat{O}\right\}$, where $|a\rangle$ and $|b\rangle$ are elements of an orthonormal basis in Hilbert space.

Of course, this is not exactly a complete description since both fields should be rather considered in a form of sum over several plain waves with different wavevectors and frequencies, but it is obvious that each term could be treated separately, because they are totally independent of each other and that is why we can afford to take just a single mode (i.e. single frequency and direction of a plane wave). We then employ the slowly varying envelope condition for the electric field, similar to the condition (3.36). In this case the time derivative of the electric field will read

$$\frac{\partial}{\partial t}\vec{E}(\vec{r},t) = -i\omega\left[\vec{E}(t)\exp(i\vec{k}\vec{r} - i\omega t) - \vec{E}^*(t)\exp(-i\vec{k}\vec{r} + i\omega t)\right]. \quad (3.101)$$

Finally, the absorbed energy could be obtained after the integration over both space and time period of the experiment. The result gains the form

$$S_A(\omega,t) = 2\omega\mathrm{Im}[E^*(t)P_s(t)], \quad (3.102)$$

which we divide by the total incoming energy of the electric field

$$I = \frac{cn(\omega)\varepsilon_0}{2}\int_{-\infty}^{+\infty}\mathrm{d}t|E(t)|^2 \quad (3.103)$$

and arrive to the expression

$$S_A(\omega) = \frac{4\omega}{cn(\omega)\varepsilon_0}\mathrm{Im}\frac{\int_{-\infty}^{+\infty}\mathrm{d}tE^*(t)P(t)}{\int_{-\infty}^{+\infty}\mathrm{d}t|E(t)|^2}. \quad (3.104)$$

More frequently we would find useful the expression where instead of time electric field and polarization are the functions of frequency which could be simply done by the Fourier transform of the final equation. This enables us to define $S_{disp}(\omega)$ as follows

$$S_A(\omega) = \int_{-\infty}^{+\infty}\mathrm{d}\omega S_{disp}(\omega) \quad (3.105)$$

where

$$S_{disp}(\omega) = \frac{4\omega}{cn(\omega)\varepsilon_0}\mathrm{Im}\frac{E^*(\omega)P(\omega)}{\int_{-\infty}^{+\infty}\mathrm{d}\omega|E^*(\omega)|^2} \quad (3.106)$$

is exactly the form we were looking for.

## 3.9 Two-dimensional coherent spectroscopy

According to Eq. (3.39) electric intensity of third order non-linear signal is proportional to third order polarization, which in the language of response functions is defined by equation (3.91). Two-dimensional spectrum may be introduced as a double Fourier transform of this equation in times $t$ and $\tau$.

$$S^R_{\mathrm{2D}}(\omega_t, T, \omega_\tau) = \int_0^\infty \mathrm{d}t \int_0^{+\infty} \mathrm{d}\tau S^{(R)}(t, T, \tau) \exp(i\omega(t-\tau) \exp(i\omega_t t - i\omega_\tau \tau)$$

where $S^{(R)} = \tilde{R}_2(t, T, \tau) + \tilde{R}_3(t, T, \tau)$. By doing that we obtained a plot that evolves with the delay time $T$. But this signal is not complete since it includes only rephasing Liouville pathways. As we mentioned at the end of the section 3.6 we can reverse the order of first and second pulses giving thus rise to non-rephasing part of the spectrum

$$S^{NR}_{\mathrm{2D}}(\omega_t, T, \omega_\tau) = \int_0^\infty \mathrm{d}t \int_{-\infty}^{+\infty} \mathrm{d}\tau S^{(NR)}(t, T, -\tau) \times$$

$$\times \exp\left(i\omega(t-\tau)\right) \exp(i\omega_t t - i\omega_\tau \tau), \tag{3.107}$$

with $S^{(NR)} = \tilde{R}_1(t, T, -\tau) + \tilde{R}_4(t, T, -\tau)$. Total spectrum is given by the sum of these two contributions. But very similarly we can proceed in defining pump-probe spectrum. Again, Eq. (3.106) shows that pump-probe spectrum is proportional to polarization

$$S_{\mathrm{PP}}(\omega, T) \approx \mathrm{Im}[E(\omega) P(\omega, T)] \tag{3.108}$$

Here, in the first approximation we make the assumption that the electric field in time domain has the form of ultrafast pulse and could be expressed as delta function, i.e. $E(t) = \delta(t)$, which makes it a constant in frequency domain, $E(\omega) = const$. This means that we can calculate pump-probe signal as an imaginary part of frequency dependent polarization, while the Fourier transformation has been applied only to the variable $t$. The delay time $\tau$ is considered to be zero in this case, which reduces the first two pulses to one. Substituting (3.91) into the last expression we get

$$S^R_{\mathrm{PP}}(\omega, T) \approx \mathrm{Im}[P(\omega, T)] \approx -\mathrm{Im}\left[iS^{(R)}(\omega_t, T, 0) \exp(i\omega_{eg} t) \exp(i\omega_t t)\right] =$$

$$= \mathrm{Re}\left[S^{(R)}(\omega_t, T, 0) \exp(i\omega_{eg} t) \exp(i\omega_t t)\right] \tag{3.109}$$

and analogically for non-rephasing signal

$$S_{\mathrm{PP}}^{NR}(\omega) \approx -\mathrm{Im}\left[iS^{(NR)}(\omega_t, T, 0)\exp(i\omega_{eg}t)\exp(i\omega_t t)\right] =$$

$$= \mathrm{Re}\left[S^{(NR)}(\omega_t, T, 0)\exp(i\omega_{eg}t)\exp(i\omega_t t)\right] \tag{3.110}$$

Now it is evident that qualitatively pump-probe spectrum is identical with real part of 2D spectrum with a condition $\tau = 0$ that reduces reduces two-dimensional spectrum to one-dimensional. Besides, it could be proved that if we integrate 2D spectrum along the $\omega_\tau$ axis we obtain pump-probe as well. Another obvious observation lies in the fact that any additional information connected with 2D spectra when compared to pump-probe comes mainly from the shape of its peaks because changes in their magnitude are usually noticeable in one-dimension too.

# Chapter 4

# NOSE Simulations

Program NOSE[1] is a computational package developed in Fortran with an interface in Tcl language. It originated in the year 2005 and since then it has been equipped with many subprograms that are able to calculate various spectra including absorption and fluorescence spectra, circular dichroism, photon echo or two-dimensional spectra. The communication with user is realized through the command line and two input files, the configuration file (.conf) and the .ssf file. In the configuration file it is necessary to specify the output of the program and to insert the corresponding .ssf file name, in addition to that it is also possible to modify experimental conditions here (i.e. to set the temperature). The parameters of the system of our interest are all included in the .ssf file. In my Bachelor's thesis [13] I made a thorough description of both main files and there is also a manual available at the webpage of the project `http://nose-project.sourceforge.net`. Once NOSE is installed on a computer it is really easy to use, since the only thing one has to do is to type 'nose' and the name of the configuration file.

The idea of this work is to compare two non-linear spectroscopic methods, the pump-probe technique and 2D spectroscopy. The main conclusion should be whether the information each method provides are comparable, or if one of the methods gives any extra pieces of information that are not apparent from the other one. The special attention will be devoted to electronic coherences, the phenomenon that has been recently observed in 2D spectroscopy (see Ref. [14]). From our simulations we will try to determine whether these effects are also included in pump-probe. These two methods have many things in common, both are performed as pulsed experiments

[1] The abbreviation stands for NOnlinear Spectroscopy (made) Easy.

with femtosecond resolution and both are meant to reveal dynamical processes in the system. Even their definitions look quite similar.

In the next three sections of this chapter we developed three exemplary situations, each one of them describing some different aspect of the spectral behavior. In the first we brought our attention to the process of relaxation, whereas the other two deal with electronic coherences.

## 4.1 Relaxation

By relaxation we mean population transfer from higher to lower excited state that is manifested in 2D spectrum by redistribution of peaks' amplitudes and positions. Population peaks are those on the main diagonal, while the off-diagonal peaks always reveal the existence of resonance coupling or relaxation between particular states. In our example we excited a coupled two-level system, with transition energies at 9600 $\mathrm{cm}^{-1}$ and 10000 $\mathrm{cm}^{-1}$, with a spectrally infinitely broad pulse and for delay time $T = 0\,\mathrm{fs}$ we could see that the majority of population resides at the higher excited state as is shown by Fig. 4.1. With an increasing delay time we can observe that the population peak at 10000 $\mathrm{cm}^{-1}$ gradually fades and in the same time there is a build-up of the crosspeak in the right bottom corner of the spectrum. This scenario may be followed by looking at the pictures 4.2-4.5. Although the differences are not so demonstrative the population peak corresponding to the lower excited state clearly increases in intensity as well. These facts confirm the existence of relaxation dynamics. The last thing worth mentioning is the presence of negative contributions for times $T = 0\,\mathrm{fs}$ and $T = 700\,\mathrm{fs}$, which are attributed to excited state absorption (ESA).

Let us now have a look at what happens in the pump-probe spectrum, which is plotted in the Fig. 4.6. The first peak at approx. 9400 $\mathrm{cm}^{-1}$increases its height during the investigated time period more than twice and the reduction of the second peak at 10000 $\mathrm{cm}^{-1}$ is also quite significant, from which could be immediately made a conclusion that both 2D spectroscopy and pump-probe technique are methods that are sensitive to population transfer. Interesting thing on this spectrum is that the biggest change of second peak's magnitude takes place during the first 350 fs, while the first peak remains almost exactly the same. This may evoke a question where the population from the higher excited state goes. The best explanation of this problem seem to be the fact that for short times there are still serious

effects of electronic coherences that has to be taken into account.

In the Fig. 4.7 the positions of maxima of both peaks from pump-probe spectrum 4.6 as a functions of delay time $T$ are plotted. When we fitted these dependencies with single exponential curves we found that they exhibit the same kinetics with the same rate constants, which determine the relaxation time. A little more problematic might seem the idea of extracting the same piece of information from 2D spectrum where we have twice as many peaks then in pump-probe. In this case we would have to select the relaxation crosspeak to obtain the same result. The other important feature of the figure 4.7 is the clear presence of oscillations for very short times under 100 fs which could be attributed to electronic coherences. The detail of this effect is shown by the Fig. 4.8.

Let us now go on to our second example where electronic coherences have been investigated under conditions where no relaxation takes place. Thus we were able to study this interesting phenomenon in its pure form, relatively isolated from other effects.

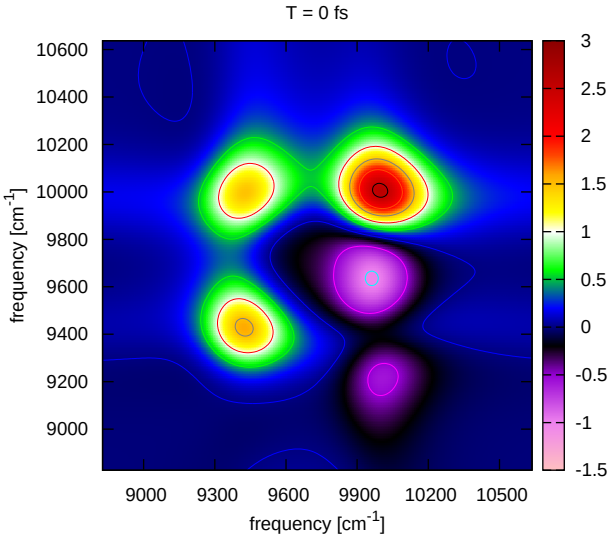


Figure 4.1: 2D correlation spectrum of relaxation between two excited states at time $\boxed{T = 0\,\mathrm{fs}}$

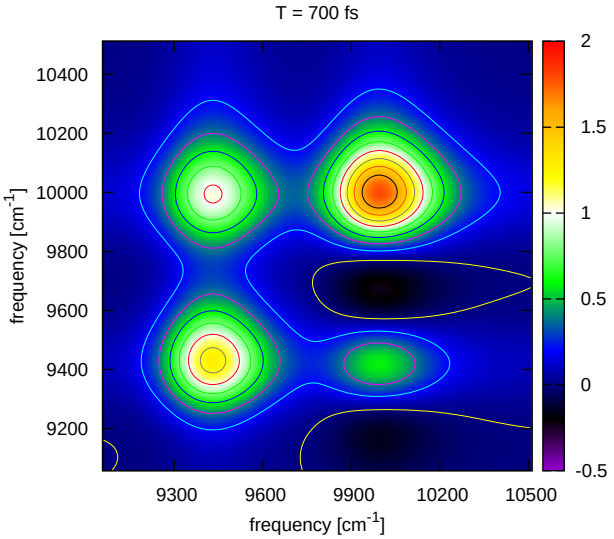


Figure 4.2: 2D correlation spectrum of relaxation between two excited states at time $\boxed{T = 700\,\mathrm{fs}}$

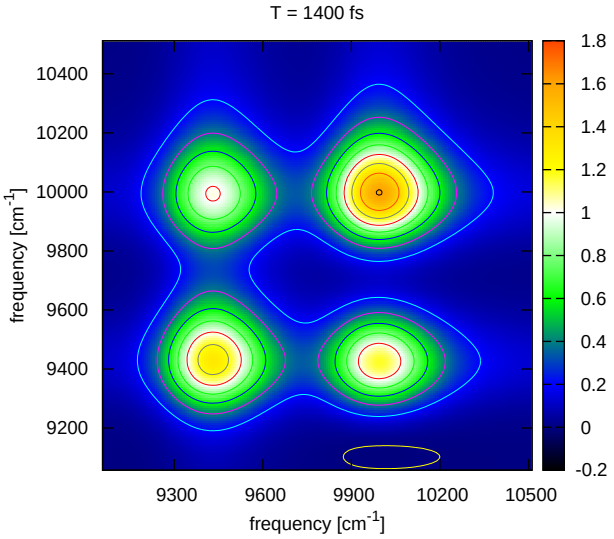


Figure 4.3: 2D correlation spectrum of relaxation between two excited states at time $\boxed{T = 1400\,\mathrm{fs}}$

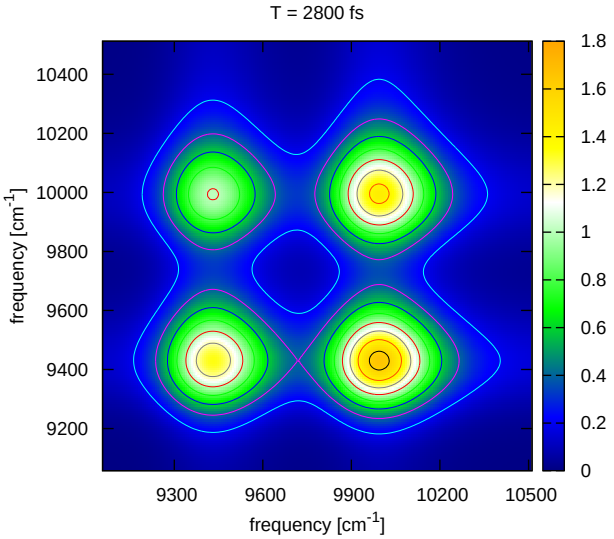


Figure 4.4: 2D correlation spectrum of relaxation between two excited states at time $\boxed{T = 2800\,\mathrm{fs}}$

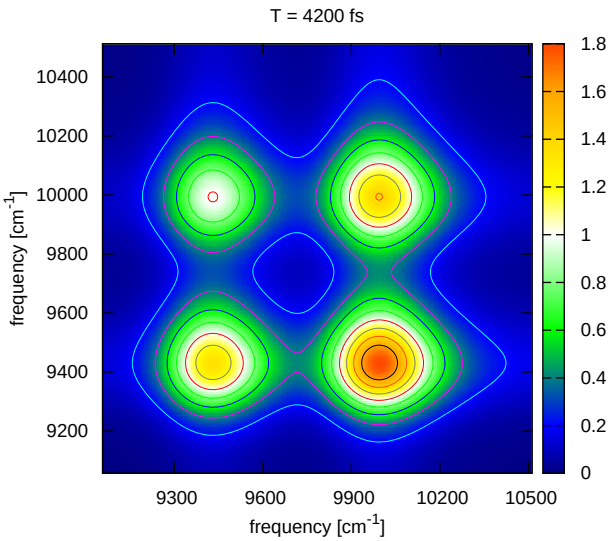


Figure 4.5: 2D correlation spectrum of relaxation between two excited states at time $\boxed{T = 4200\,\mathrm{fs}}$

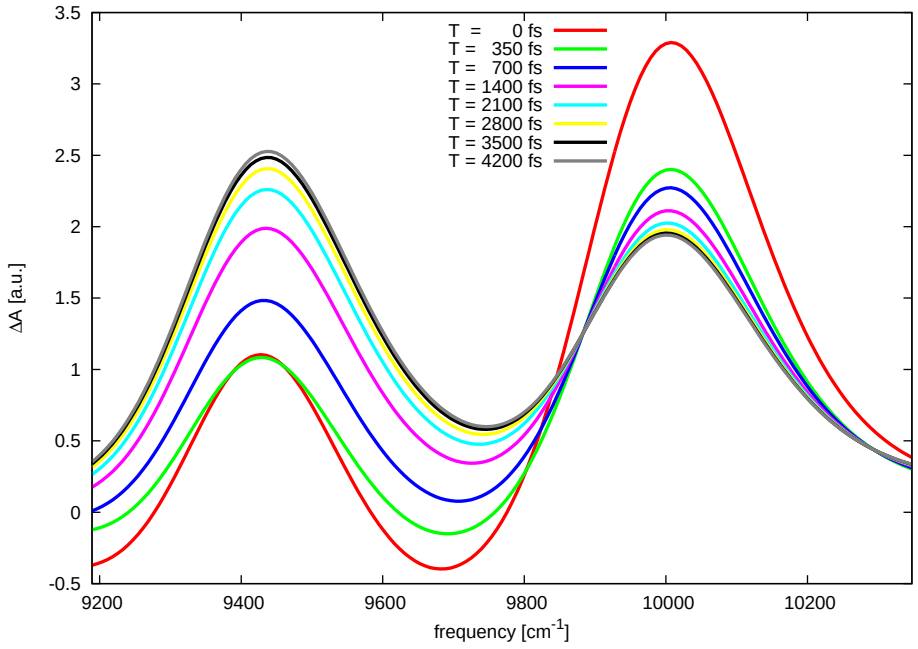


Figure 4.6: Pump-probe spectrum of the relaxation between two excited states for delay times from $T = 0\,\mathrm{fs}$ to $T = 4200\,\mathrm{fs}$.

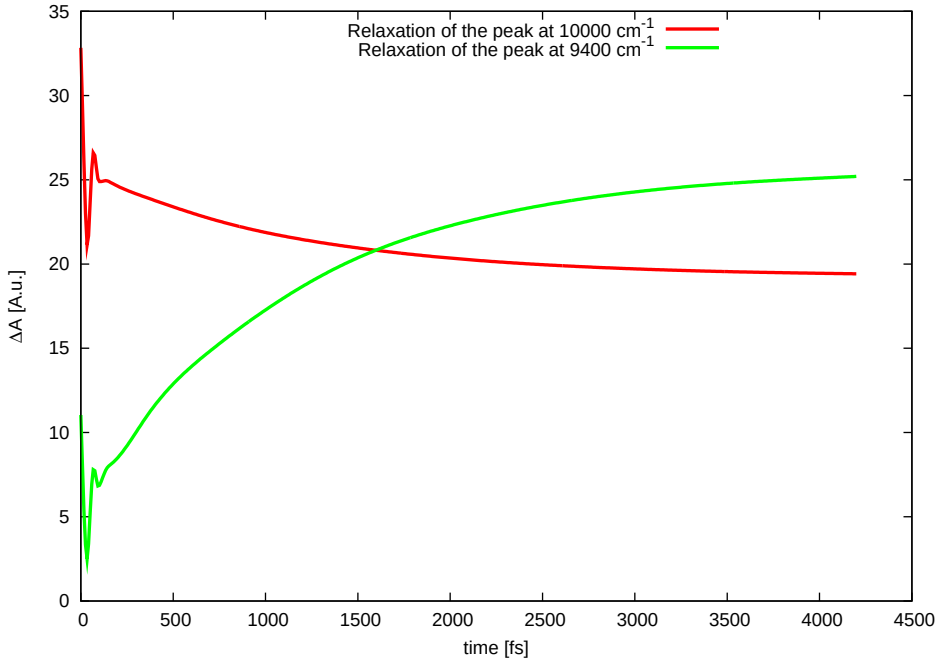


Figure 4.7: The process of relaxation from Fig. 4.6.

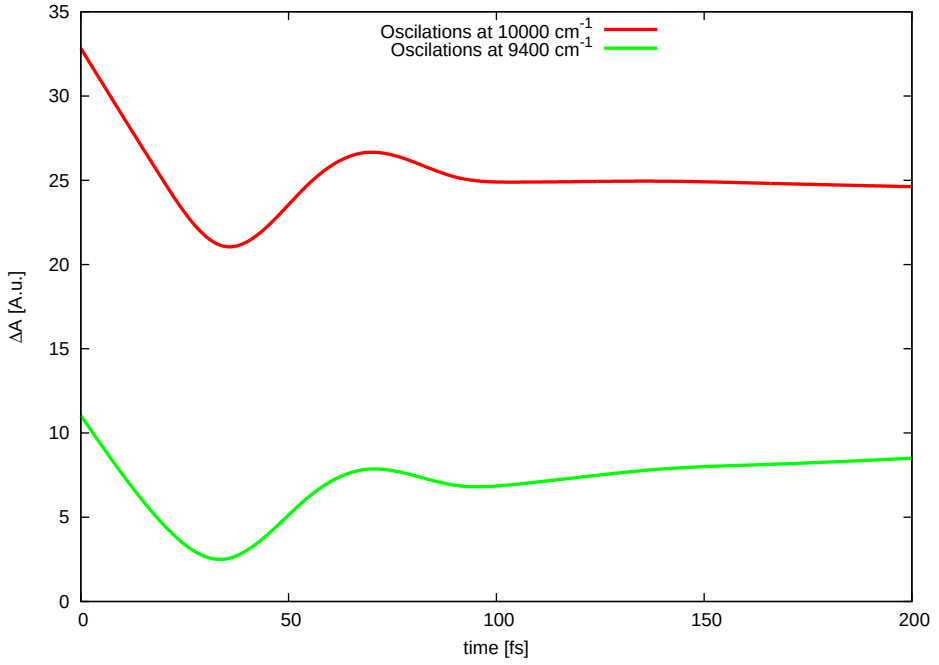


Figure 4.8: Detail of the oscillations from Fig. 4.7

## 4.2 Electronic coherences in the system with strong coupling

The effect of electronic coherences and their manifestation in non-linear spectra is not yet fully understood and lacks clear interpretation. We again supposed a model system with electronic transitions on 9600 $cm^{-1}$ and 10000 $cm^{-1}$, but this time with strong coupling between excited electronic states and with no relaxation effects taking place in the background.

In 2D spectra the most distinctive characteristic that reveals the presence of electronic coherences are the changes in the orientations of its crosspeaks. We simulated our system's behavior for seven different delay times $T$. Starting with $T = 0\,\text{fs}$, in the picture 4.9 we see that crosspeaks are oriented in the direction of this arrow $\nearrow$, i.e. the direction is the same as that of the main diagonal of the two-dimensional plot. As we proceed in time the crosspeaks change their orientation and their shapes becomes quite rounded (Fig. 4.10). We will designate this stage of the peak by the arrow $\uparrow$. For $T = 18\,\text{fs}$ (Fig. 4.12) the orientation becomes opposite to that in $T = 0\,\text{fs}$, which we represent by the arrow $\nwarrow$. It is evident from the sequence of the pictures 4.9-4.15 that the crosspeaks directions evolve in this fashion $\nearrow - \uparrow - \nwarrow - \uparrow - \nearrow - \uparrow - \nwarrow$. But it is not only orientation of the crosspeaks that changes, it is their height. For times $T = 18\,\text{fs}$ and $T = 54\,\text{fs}$ (the $\nwarrow$ orientation) the peaks are much less intense than those in times $T = 0\,\text{fs}$ and $T = 36\,\text{fs}$ (the $\nearrow$ orientation). This suggest that we should be able to observe electronic coherences in pump-probe spectra as well and in this case this is really true.

This fact is demonstrated in Fig. 4.16 where are pump-probe spectra of all necessary delay times. As expected the peaks corresponding to $T = 0\,\text{fs}$ and $T = 36\,\text{fs}$ are approximately twice as high as the peaks corresponding to $T = 18\,\text{fs}$ and $T = 54\,\text{fs}$. This is an interesting result, since in natural molecular systems studied in real spectroscopic experiments, no such electronic coherences manifestation in pump-probe spectra have been observed so far. The reason for this of course could be in different experimental conditions and also in the fact that real systems are more complex than a simple two-level system. That is why in our third example we tried to find such parameters of the system that would represent real molecular systems in the most plausible way.

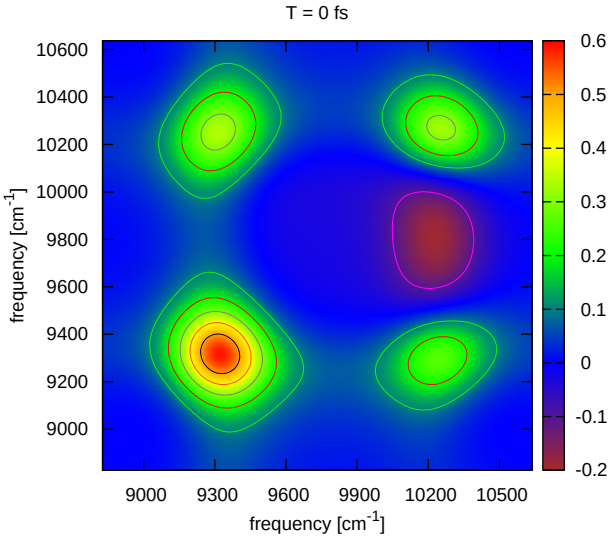


Figure 4.9: 2D correlation spectrum of two strongly coupled excited electronic states at time $\boxed{T = 0\,\text{fs}}$. The crosspeak orientation is $\nearrow$.

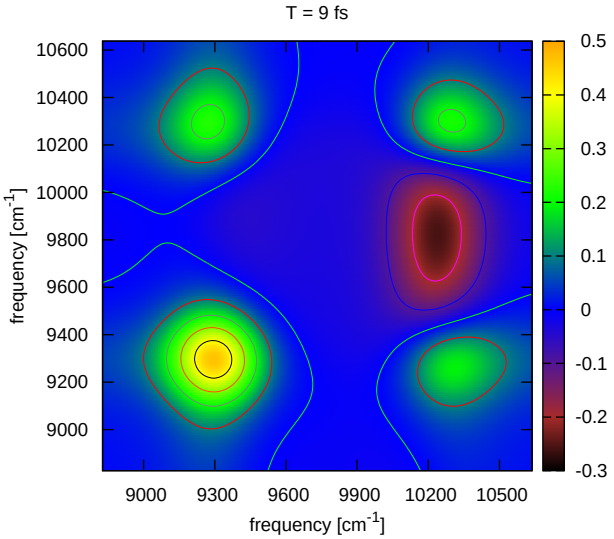


Figure 4.10: 2D correlation spectrum of two strongly coupled excited electronic states at time $\boxed{T = 9\,\text{fs}}$. The crosspeak orientation is $\uparrow$.

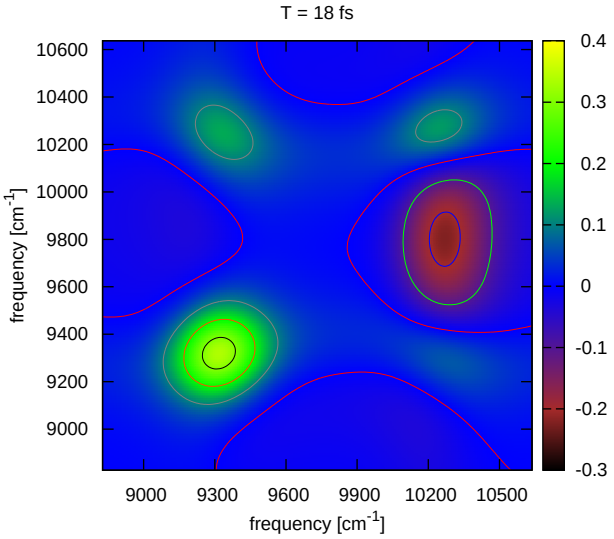


Figure 4.11: 2D correlation spectrum of two strongly coupled excited electronic states at time $\boxed{T = 18\,\mathrm{fs}}$. The crosspeak orientation is $\nwarrow$.

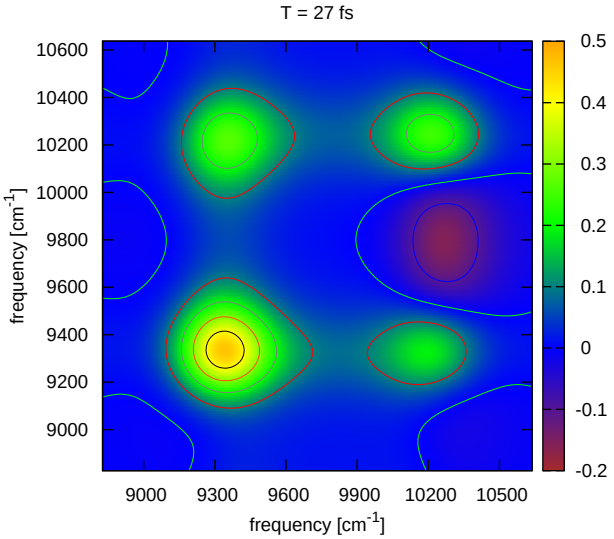


Figure 4.12: 2D correlation spectrum of two strongly coupled excited electronic states at time $\boxed{T = 27\,\mathrm{fs}}$. The crosspeak orientations is $\uparrow$.

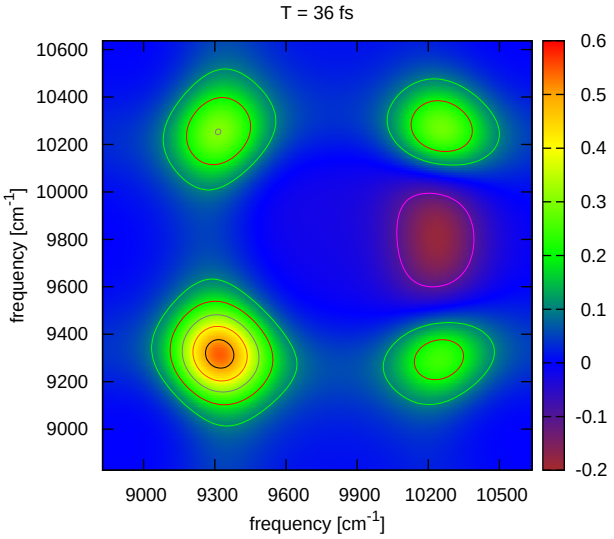


Figure 4.13: 2D correlation spectrum of two strongly coupled excited electronic states at time $\boxed{T = 36\,\mathrm{fs}}$. The crosspeak orientation is ↗.

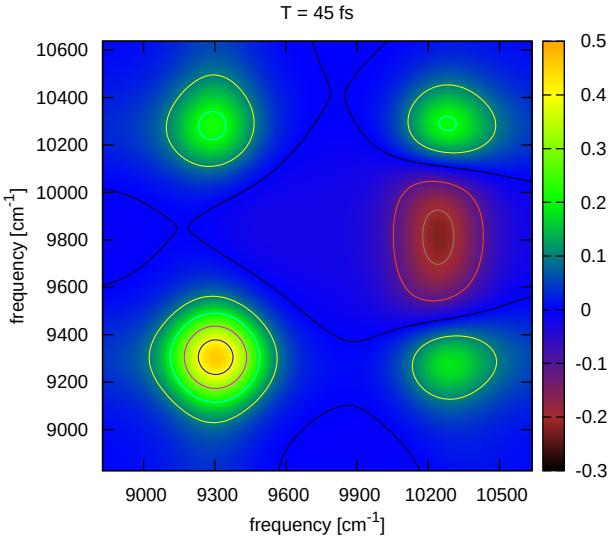


Figure 4.14: 2D correlation spectrum of two strongly coupled excited electronic states at time $\boxed{T = 45\,\mathrm{fs}}$. The crosspeak orientation is ↑.

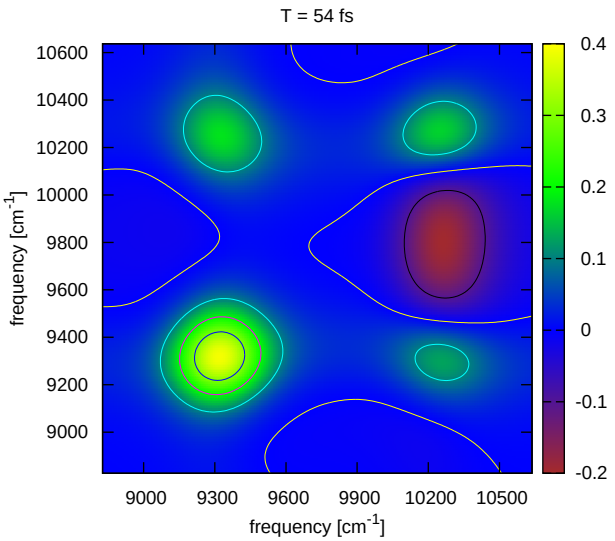


Figure 4.15: 2D correlation spectrum of two strongly coupled excited electronic states at time $\boxed{T = 54\,\mathrm{fs}}$. The crosspeak orientation is ↖.

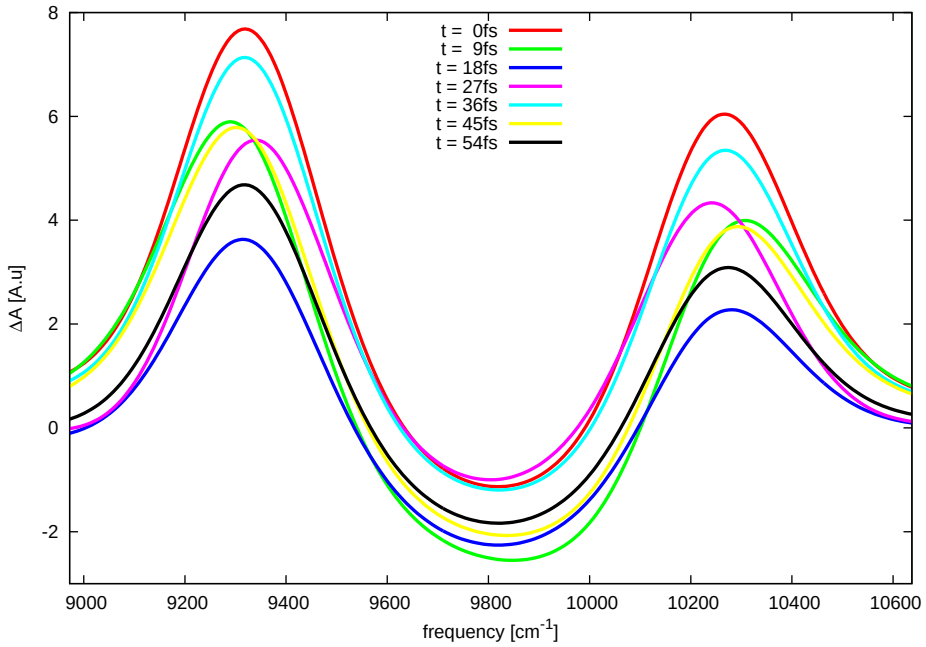


Figure 4.16: Pump-probe spectrum of two strongly coupled excited electronic states for delay times from $T = 0\,\mathrm{fs}$ to $T = 54\,\mathrm{fs}$.

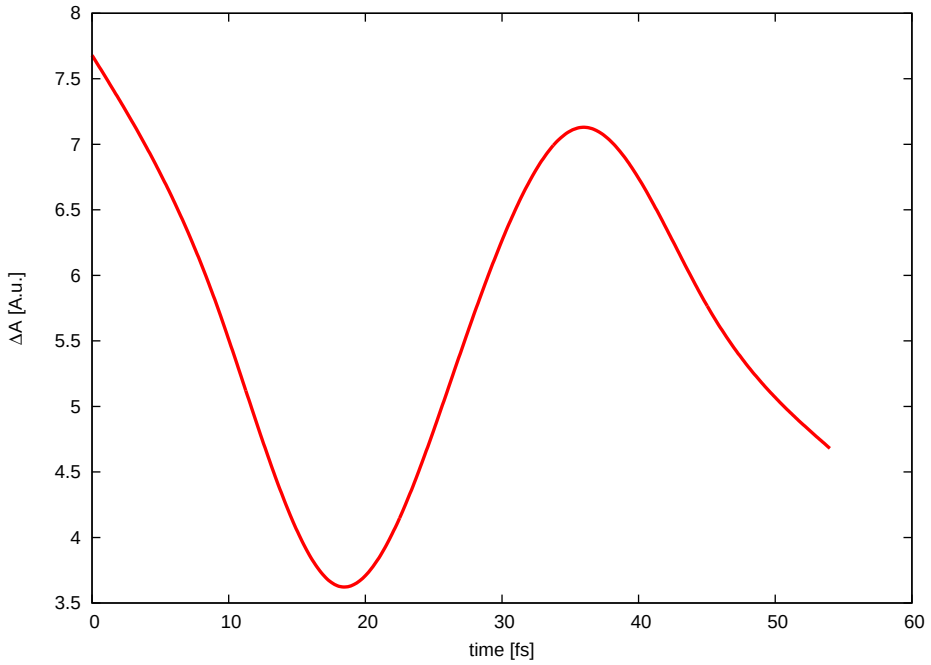


Figure 4.17: Time evolution of the 10300 $cm^{-1}$ peak magnitude for short delay times.

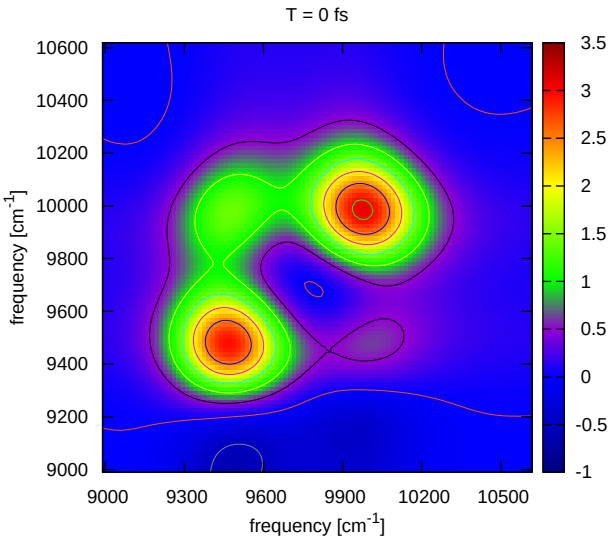


Figure 4.18: 2D correlation spectrum of two weakly coupled excited electronic states at time $\boxed{T = 0\,\text{fs}}$. The orientation of the crosspeak is ↗.

## 4.3 Weak electronic coherences

As in previous examples we suppose a two-level system with electronic transitions at 9600 $\text{cm}^{-1}$ and 10000 $\text{cm}^{-1}$. The main difference is that this time the level of exciton coupling is considerably lower, which implies that crosspeaks are much weaker in intensity compared to populations peaks on the main diagonal. But despite this fact we should still be able to observe electronic coherences when looking at the orientation of the crosspeaks. We have no problem in doing that for delay time $T = 0\,\text{fs}$ (see Fig. 4.18). But as the system evolves it becomes more and more difficult to see the desired patterns. With a little more trouble we are able to tell the orientation of the crosspeak for time $T = 28\,\text{fs}$ (Fig. 4.20). However, in the Fig. 4.22 we can barely see anything indicative.

As for the pump-probe spectra (Fig. 4.23) we come to the very same conclusion as in the previous paragraph. There are some visible changes in the peak height up to delay times around 50 fs but after that the changes become too small. A plot of these changes is shown in the Fig. 4.24.

Hence, according to our simulations it shows up that electronic coherences should be observable in both two-dimensional spectroscopy and pump-probe experiments if the time resolution of the experiment is sufficient.

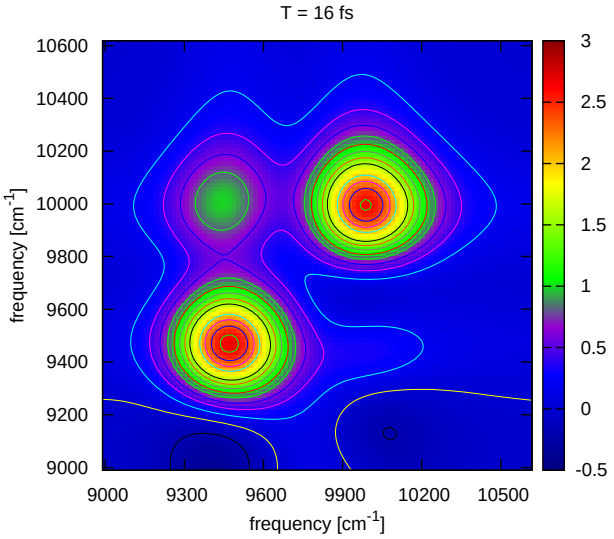


Figure 4.19: 2D correlation spectrum of two weakly coupled excited electronic states at time $\boxed{T = 16\,\mathrm{fs}}$. The orientation of the crosspeak is ↑.

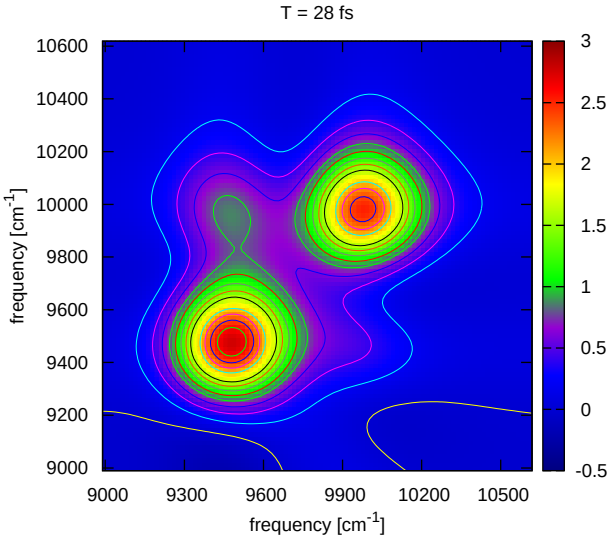


Figure 4.20: 2D correlation spectrum of two weakly coupled excited electronic states at time $\boxed{T = 28\,\mathrm{fs}}$. The orientation of the crosspeak is ↖.

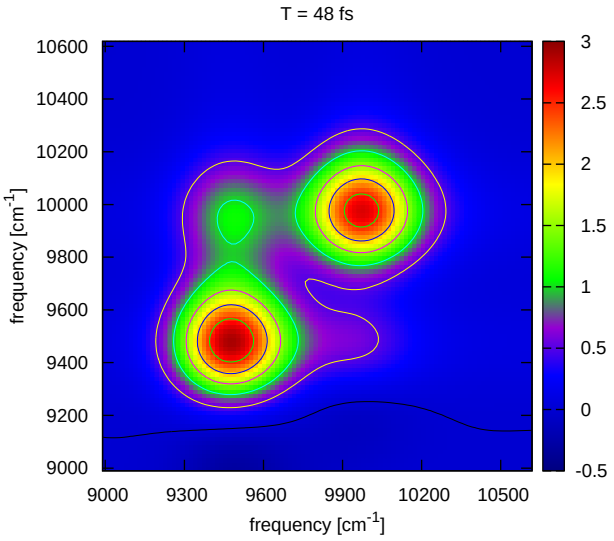


Figure 4.21: 2D correlation spectrum of two weakly coupled excited electronic states at time $\boxed{T = 48\,\mathrm{fs}}$. The orientation of the crosspeak is $\uparrow$.

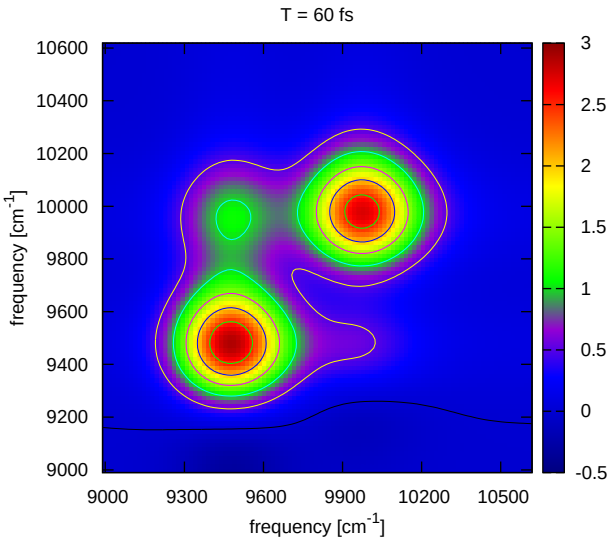


Figure 4.22: 2D correlation spectrum of two weakly coupled excited electronic states at time $\boxed{T = 60\,\mathrm{fs}}$. The orientation of the crosspeak is (should be) $\nearrow$.

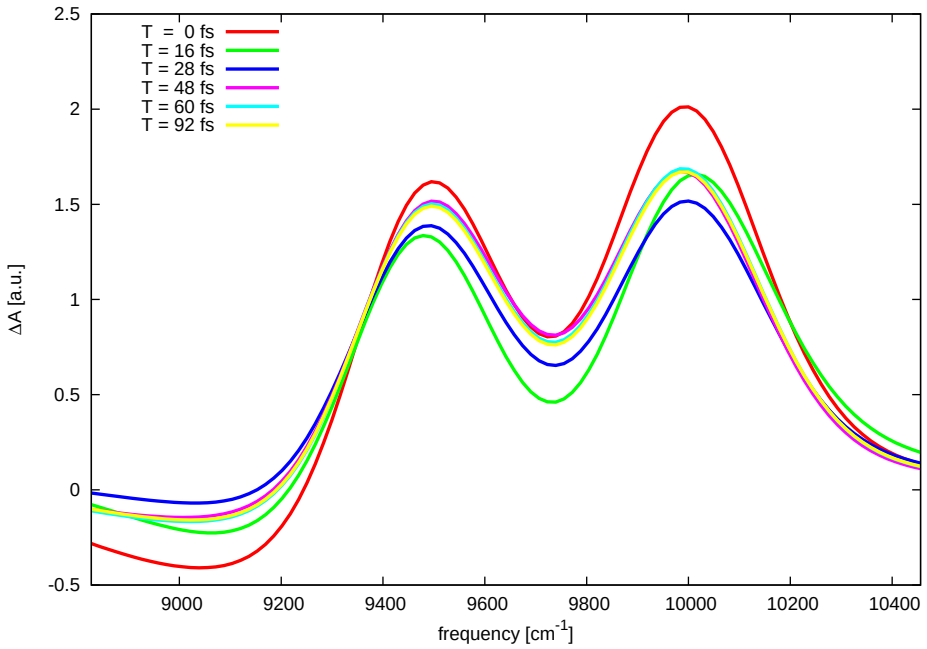


Figure 4.23: Pump-probe spectrum of two weakly coupled excited electronic states for delay times from $T = 0\,\mathrm{fs}$ to $T = 54\,\mathrm{fs}$

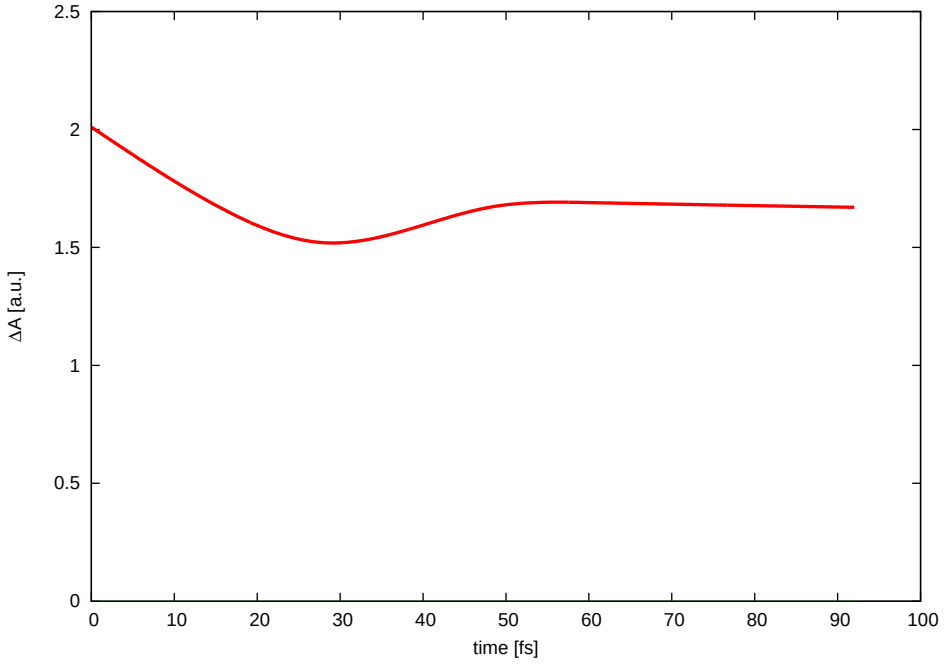


Figure 4.24: Time evolution of the 10000 $\mathrm{cm}^{-1}$ peak magnitude for short delay times.

# Chapter 5

# Conclusion

The purpose of this thesis was to provide a review of the pump-probe experimental technique and its applications to studies of molecular systems, and to perform a comparison of the pump-probe with 2D coherent spectroscopy. We also intended to set forward the fundamental concepts of the theory of non-linear response functions that has a general significance in spectroscopy, since it applies to such experiments as fluorescence up-conversion, pump-probe, two-dimensional correlation spectroscopy and other pulsed experiments. The whole work was restricted to first and third order of perturbation theory. Due to reasons of symmetry second order signal is not observed for isotropic materials. Higher orders usually do not contain any significant additional information. From the theory presented here we derived the expressions that link intrinsic properties of the studied system with measured signals. We introduced both definitions of two-dimensional spectrum and pump-probe spectrum in terms of third order response functions. After that we applied our results to analyze relaxation processes and effects of electronic coherences in two-dimensional spectra. The main goal was to decide whether are these effects also included in pump-probe spectra. Therefore, we compared data for three different theoretical systems and came to the conclusion that pump-probe contains information about electronic coherences.

The simulations were performed with help of the spectroscopic program NOSE, which is a computational package designed to calculate various kinds of spectra (absorption, fluorescence, circular dichroism). Since there was no section in the program that would be concerned with computing pump-probe I had to get familiar with the code and to add it myself. I managed to create a functional routine that gives pump-probe spectra for the case when the

excitation pulse is infinitely short, i.e. the case when the excitation is done through the all wavelengths of the spectrum. It is my goal though to include the case when excitation is spectrally localized in the future.

The three example theoretical systems we used for our simulations were quite realistic. The first one was modeled to show that both two-dimensional spectra and pump-probe are suitable to study population transfer. The results were quite consistent in this particular case. Both methods exhibited significant changes when the delay time $T$ of the incoming pulses was varied. The observation that pump-probe reveals system's populational dynamics is not new, but it served us as confirmation for the results we achieved from our theory. All of our simulations were performed with a simple two-level system with resonance coupling between the two excited states, which makes our data quite transparent.

More important were the other two simulations, which dealt with electronic coherences. That is a very interesting phenomenon observed in two-dimensional spectra. Its connection to the internal properties of the system is not yet fully clearified, but it provides the information whether the energy transport is coherent or not. However, there is not any observation up to date of electronic coherence in pump-probe. The first simulation we did in this context supposed a two-level system with strong coupling (400 $\mathrm{cm}^{-1}$) between excited states. Our data revealed that electronic coherences which take place in such a system are visible both in 2D and pump-probe. Due to the strong coupling, this was not surprising as the intensity of the crosspeaks in this case was comparable with that of population peaks. Consequently, the changes in peaks' amplitude in pump-probe were rather significant (for the lowest and highest limit cases cca. 50% of the highest peak).

The last simulation assumed a system for which the electronic coupling was considerably smaller than in the previous model (10 $\mathrm{cm}^{-1}$). As a result of this choice, the differences in intensities of population peaks and crosspeaks increased and oscillations of crosspeaks were not combined with changes in pump-probe peak amplitudes. But still we observed differences in these amplitudes (for the lowest and highest limit cases cca. 20% of the highest peak) for short delay times, cca. $T < 50\,\mathrm{fs}$. For longer times the differences vanished. However, in 2D spectra we were not able to see orientations of the crosspeaks as clearly as we expected. Just like in the pump-probe spectra, they were evident only for short delay times. The result from our simulations is thus following: Electronic coherences should be recognizable in two-dimensional coherent spectroscopy as well as in pump-probe spectra.

# Bibliography


[1] Rudi Berera, Rienk van Grondelle, John T. M. Kennis: *Ultrafast transient absorption spectroscopy: principles and application to photosynthetic systems*, Photosynth Res (**2009**) 101:105-118

[2] Y.-Z. Ma, J. Aschenbrücker, M. Miller, T. Gillbro: *Ground-state vibrational coherence in chlorosomes of the green sulfur photosynthetic bacterium Chlorobium phaeobacteroides*, Chemical Physics Letters 300 (**1999**), 465-472

[3] Michael Woerner, Flavio Zamponi, Zunaira Ansari, Jens Dreyer, Benjamin Freyer, Mirabelle Prémont-Schwarz, Thomas Elsaesser: *Concerted electron and proton transfer in ionic crystals mapped by femtosecond x-ray powder diffraction*, The Journal of Chemical Physics 133, 064509 (**2010**)

[4] Vladimir I. Novoderezhkin, Miguel A. Palacios, Herbert van Amerongen, Rienk van Grondelle: *Excitation Dynamics in the LHCII Complex of Higher Plants: Modeling Based on 2.72 Å Crystal Structure*, J. Phys. Chem. B **2005**, 109, 10493-10504

[5] Jiang Li, Zheyun Liu, Chuang Tan, Xunmin Guo, Lijuan Wang, Aziz Sancar, Dongping Zhong: *Dynamics and mechanism of repair of ultraviolet-induced (6-4) photoproduct by photolyase*, Nature, Vol 466, **2010**, 887-891

[6] Dario Polli, Piero Altoe, Oliver Weingart, Katelyn M. Spillane, Cristian Manzoni, Daniele Brida, Gaia Tomasello, Giorgio Orlandi, Philipp Kukura, Richard A. Mathies, Marco Garavelli, Giulio Cerullo: *Conical intersection dynamics of*

*the primary photoisomerization event in vision*, Nature, Vol 467, **2010**, 440-443

[7] Rienk van Grondelle, Vladimir I. Novoderezhkin: *Energy transfer in photosynthesis: experimental insights and quantitative models*, Phys. Chem. Chem. Phys., **2006**, 8. 793-807

[8] Matthijs R. Panman, *et. al.*: *Operation Machanism of a Molecular Machine Revealed Using Time-Resolved Vibrational Spectroscopy*, Science 328, 1255 (**2010**)

[9] William A. Tisdale, *et. al.*: *Hot-Electron Transfer from Semiconductor Nanocrystals*, Science 328, 1543 (**2010**)

[10] Josh Vura-Weis, *et. al.*: *Crossover from Single-Step Tunneling to Multistep Hopping for Molecular Triplet Energy Transfer*, Science 328, 1547 (**2010**)

[11] Shaul Mukamel: *Principles of Nonlinear Optical Spectroscopy*, Oxford University Press, 1995

[12] Wolfgang Demtröder: *Laser Spectroscopy*, 3rd Edition, Springer, 2003

[13] Jan Linhart: *Structure and Spectra of Photosynthetic Reaction Centers*, Bachelor's thesis, Faculty of Mathematics and Physics of Charles University, The Institute Of Physics, 2009 (In Czech)

[14] Gregory S. Ensel, Tessa R. Calhoun, Elizabeth L. Read, Tae-Kyu Ahn, Tomáš Mančal, Yuan-Chung Cheng, Robert E. Blankenship, Graham R. Fleming: *Evidence for wavelike energy transfer through quantum coherence in photosynthetic systems*, Nature, Vol 446, **2007**, 782-786